1-D modelling of the sedimentation process in the hopper

A 1-D cross section averaged flow model to predict the cargo distribution and overflow losses of sand in a Trailing Suction Hopper Dredger

by

J. Boone

Delft University of Technology

Section of Dredging Engineering

In association with

Van Oord Dredging and Marine Contractors

November 8th , 2016

1-D modelling of the sedimentation process in the hopper

Author:
Boone J. (Jordy)

Thesis Committee:
Delft University of Technology
Prof.Dr. ir. C. van Rhee
Dr. ir. G.H. Keetels
Dr.ir. P.E. Wellens

Van Oord Dredging and Marine Contractors
Dr.ir. M.A.J. de Nijs

In association with:
Van Oord Dredging and Marine Contractors

Acknowledgements

Writing a MSc-thesis is the last part of the curriculum to achieve the Master in Science degree in Offshore and Dredging Engineering at Delft University of Technology.

The last 10 months of my Masters I was working on the development of a numerical model to simulate the sedimentation process arising inside the hopper. This graduate topic was proposed by Dr.ir. M.A.J. de Nijs, Manager at the Research and Development department at Van Oord Dredging and Marine Contractors.

I would first like to thank my supervisor Dr.Ir. M.A.J. de Nijs of Van Oord Dredging and Marine Contractors for providing me motivating feedback, the possibility to discuss difficulties and the support during this graduation project. I really appreciate the advice and support during my graduation period.

From the Delft University of Technology, I thank Prof. Dr. Ir Cees van Rhee and Dr.Ir. Geert Keetels for their critical evaluation of my work, their advice and the possibility to discuss problems.

Finally, I must express my very profound gratitude to my girlfriend Aline, my parents and friends for providing me with unfailing support throughout my years of study and through the period of graduation. Thank you.

Jordy Boone
November 8th , 2016

Abstract

The total overflow losses during dredging activities determines the loading performance of Trailing Suction Hopper Dredgers. Therefore, predictions of the hopper sedimentation process in advance enables improvement of the effectiveness of the loading process and hence of the profitability of the TSHD.

Previous models on the hopper sedimentation process include hopper volume averaged frameworks, one-dimensional vertical (1DV) and two-dimensional vertical along the hopper (2DV) models. However, these models do not include horizontal transport variation (1DV) and the variation of the cross-sectional hopper shape (1DV & 2DV).

The objective of this research was to develop a new sedimentation model to provide predictions of the overflow losses and the sandy-cargo distribution inside the hopper and to include variations of the cross-sectional shape of the hopper. The model conceptualised in this thesis intends to provide a practical working tool that balances the need for inclusion of the related physical processes and computational time and complexity. The approach has therefore been to incorporate more physical processes than in 1DV models but do not meet the complexity of a 2DV model.

To this end, this thesis describes the development of a two-layered 1D cross-section averaged numerical model which solves the layer averaged shallow water equations to predict the transport of sand. The model considers horizontal advection of water and sediment within a cross-section averaged framework that includes the geometrical variation of the hopper cross-section. Previous research shows that density currents plays a major role in the hopper sedimentation process. Therefore, the hydrodynamic model has been divided into two currents, an external driven free surface flow and a density driven internal flow. These hydrodynamic models has been dynamically coupled with the bed profile through erosion and deposition of sediment. Vertical transport between the two flows includes sediment settling, upward flow and entrainment effects.

Verification to idealised analytical solutions demonstrated that the hydrodynamic numerical models for the external and internal flow are mass, momentum and energy conservative. Furthermore the discretised models are robust and can deal with high and low (internal) Froude number flows and drying and flooding phenomena without the need of particular case specific numerical settings.

Laboratory experiments have been used for model calibration and an independent set of measurements for model validation. It is demonstrated that although a model of the external (barotropic) flow can predict the (overflow) losses well, the horizontal transport by turbidity currents has to be included to correctly predict longitudinal cargo distribution. Validation of the model against prototype overflow loss measurements showed similar order of magnitude predictions.

Therefore, this study demonstrates that the developed model predicts the amount of overflow losses and the longitudinal bed level elevation on model and prototype scale favourably well at a low user complexity level and requiring low computational time.

Contents

Nomenclature

Roman Symbols

A_b	Cross − section averaged bed area	$[m^2]$
A_e	Cross − section external flow area	$[m^2]$
A_i	Cross − section averaged internal flow area	$[m^2]$
A_{ov}	Overflow profile	$[m^2]$
B	Hopper width	$[m]$
c_b	Settled bed concentration	$[-]$
c_e	External layer concentration	$[-]$
C_D	Drag coefficient	$[-]$
c_i	Internal layer concentration	$[-]$
c_{in}	Inflow concentration	$[-]$
c_{ov}	Overflow concentration	$[-]$
D	Grain diameter	$[m]$
D_{ov}	Diameter of the overflow	$[m]$
D_*	Dimensionless particle diameter	$[-]$
D_{dep}	Deposition flux	$[kg/m^2s]$
E	Pick − up flux	$[kg/m^2s]$
f_0	Friction factor for sand	$[-]$
F_r	Froude number	$[-]$
g	Gravitational acceleration	$[m/s^2]$
h	Internal layer height	$[m]$
H	Total flow height	$[m]$
h_{up}	Water layer above overflow level	$[m]$
k	permeability	$[m^2]$
L	Hopper length	$[m]$
M	Solids mass	$[kg]$
n_0	Bed porosity	$[-]$
OV_{cum}	Cumulative overflow loss	$[-]$
p	Pressure	$[N/m^2]$
P	Length of wetted perimeter	$[m]$
$P_{E,\phi}$	Solids entrainment	$[kg/m^2s]$
$P_{lp,\phi}$	Solids discharge flux	$[kg/m^2s]$
$P_{lp,w}$	Water discharge flux	$[kg/m^2s]$
$P_{ov,\phi}$	Solids overflow flux	$[kg/m^2s]$
$P_{ov,w}$	Water overflow flux	$[kg/m^2s]$
Q_{in}	Mixture discharge into the hopper	$[m^3/s]$
Q_{ov}	Overflow discharge	$[m^3/s]$
R_p	Particle reynolds number	$[-]$
t	time	$[s]$
U_e	external flow velocity	$[m/s]$
U_i	internal flow velocity	$[m/s]$
v_e	Erosion velocity	$[m/s]$
v_s	slip velocity	$[m/s]$
v_{sed}	sedimentation velocity	$[m/s]$
v_w	Upward water velocity	$[m/s]$

w_0	settling velocity single grains	$[m/s]$
w_s	Hindered settling velocity	$[m/s]$
z	Bed level	$[m]$

Greek symbols

α	Distribution coefficient	$[-]$
β	Distribution coefficient	$[-]$
Δ	Specific density $(\rho_s - \rho_w)/\rho_w$	$[-]$
E	Relative density $(\rho_i - \rho_e)/\rho_i$	$[-]$
ϕ_e	External concentration	$[-]$
ϕ_i	Internal concentration	$[-]$
ϕ_{inflow}	Inflowing mixture concentration	$[-]$
μ	Overflow coefficient	$[-]$
ν	Kinematic viscosity	$[m^2/s]$
θ	Shields parameter	$[-]$
θ_{cr}	Critical shields parameter	$[-]$
ρ	Density	$[kg/m^3]$
ρ_b	bed density	$[kg/m^3]$
ρ_e	external layer density	$[kg/m^3]$
ρ_m	mixture density	$[kg/m^3]$
ρ_i	internal layer density	$[kg/m^3]$
ρ_s	solids density	$[kg/m^3]$
ρ_w	water density	$[kg/m^3]$
τ	shear stress	$[N/m^2]$
τ_b	bed shear stress	$[N/m^2]$
τ_i	Interface shear stress	$[N/m^2]$
ξ_e	water level	$[m]$

List of Figures

List of Tables

1 Introduction

1.1 General

Trailing suction Hopper Dredgers (TSHD) are commonly used in the dredging industry at a wide variety of maintenance, land reclamation and maritime construction projects. During dredging operations the TSHD trails a draghead over the seabed to suck up materials like sand, clay or gravel. The dredged mixture is discharged into the ship's cargo hold (hopper) where the particles settle and form a sediment bed. Consequently the surplus of water in the hopper flows back overboard through the overflow when the water level inside the hopper exceeds the overflow level. However, this overflowing water can contain fractions of non-settled sediments which consequently results in a loading production lower than the suction production. Prediction of this particular sedimentation process is of great interest to provide predictions of the loading efficiency (amount of overflow losses) and the cargo distribution along the hopper length.

Several researchers investigated the sedimentation process in Trailing Suction Hopper Dredgers. As a result several mathematical approaches exist to simulate the hopper sedimentation processes. One of the first models developed to simulate hopper sedimentation processes is Camp's point model (Camp, 1946). Several other researchers have developed more process-based 1DV and analytical models (Vlasblom & Miedema, 1995), (van Rhee, 2002), (Spearman, 2014). These 1DV and 2DV models include flow and transport variation in the vertical (1DV & 2DV) and in the horizontal (2DV).

1.2 Problem definition and aim of this study

Previous developed models provide reasonable values concerning the overflow losses but at the same time they all have their advantages and disadvantages. They do not all include the bed level variation along the hopper. Furthermore, most models (except 2DV) do not include transport variation in the horizontal or are based on simplified uniform or logarithmic horizontal velocity distributions (Camp, 1946), (Spearman, 2014) and do not include density currents. Hence, due to the lack in horizontal transport variation, these models cannot provide predictions of the (variable) cargo distribution along the hopper. Furthermore the existing models do not include cross-sectional hopper shape and inflow/overflow systems are simplified. Moreover the models (1DV & 2DV) cannot deal with drying and flooding phenomena which can occur when e.g. the overflow is lowered. The shortcomings of the existing models and the demand for a more process-based model to predict the overflow losses and cargo distribution along the hopper resulted in a new model approach.

This thesis aims at developing a robust and practical working tool which includes relevant physical processes to provide sound physical predictions of longitudinal distribution of the hopper cargo and amount of overflow losses. The model should include the effects of density currents, variation of cross-sectional shape of the hopper and has to perform at a low (user) complexity level and with faster calculation speed than a 2DV model. Therefore, this model approach includes horizontal advection processes in contrast to point or 1-DV models. This enables the mathematical description of density current transport and longitudinal distribution of hopper cargo

within a 1-D cross-sectional averaged framework to limit the computational time and complexity level.
The model should allow the user to specify different hopper cross-section shapes i.e. keelson or silo hopper cross-sectional shapes. Discharge and overflow positions/configuration along the hopper length should be variable to simulate different loading strategies.

The objective as described above results in the following research question:

Can a two-layered 1D horizontal numerical model within a cross-sectional framework provide valid predictions for the amount of overflow losses and longitudinal cargo distribution?

1.3 Research methodology and thesis set up

First a literature study has been performed to investigate the processes and performance of the existing sedimentation models. Based on the shortcomings of those models a new model approach has been proposed. Thereafter the conceptualised model is sketched to describe the relevant physical processes arising in the hopper (Chapter 2. Secondly the mathematical framework (governing differential equations) to describe the barotropic (external) and baroclinic (internal) flows are derived based on cross-sectional averaged conservation of mass and momentum (Chapter 3). Chapter 4 formulates the closure relations to close the set of differential equations as derived in Chapter 3. The closure relations define the water and sediment exchange fluxes as well as the inflow and overflow conditions.

The numerical scheme is discretised with a Finite Volume approach with upwind advection flux discretisation and the Euler method for time discretisation on a staggered grid (Chapter 5). Thereafter the specific parts of the hydrodynamic model are verified against a number of idealised analytical solutions (Chapter 6) such as dam breaks, hydraulic jumps and lock exchange flows. Both hydrodynamic models (barotropic and baroclinic flow) are extensively verified against the analytical solutions.

The developed sedimentation model is calibrated and validated against laboratory experiments and prototype measurements (Chapter 7). Firstly only the external (barotropic) flow is compared with the measured results and thereafter the effects of density currents is included. Furthermore the calibrated model is verified against a prototype measurement to show the model performance on prototype scale. Finally conclusions and recommendations are presented in Chapter 8 & 9.

2 Sedimentation processes in the Trailing Suction Hopper Dredger

This chapter introduces the relevant physical processes concerning suspended sediment transport arising inside the hopper during hopper filling. First a short overview of the working principle of the Trailing Suction Hopper Dredger is presented. Secondly existing hopper sedimentation models are summarised and the shortcomings of these models is mentioned. At the end of this chapter the motivation for the development of a new model approach to describe the hopper sedimentation process is formulated based on the shortcomings of the existing models. Finally the proposed conceptual model with the relevant physical processes is described.

2.1 Introduction dredging process

Trailing suction hopper dredgers are self-propelled ships that contain a cargo hold (hopper) and which are equipped with one or two suction pipes, see Figure 2.1. Dragheads attached to the suction pipes act like giant vacuum cleaners and they are primarily used to suck up materials like sand, clay or gravel.

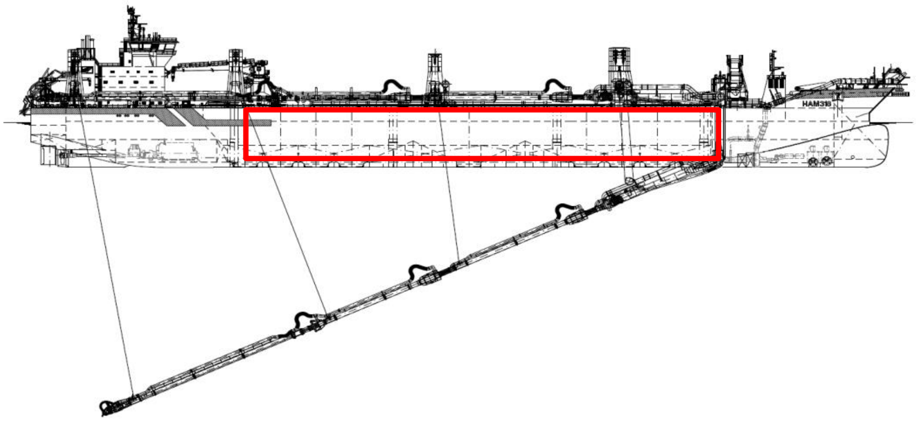

Figure 2.1: Overview of a Trailing suction hopper dredger.

During dredging the ship trails the draghead(s) over the seabed and sucks up a water-sediment mixture. The mixture is hydraulically transported through the suction pipes towards the cargo hold, the hopper, were the discharged sediment settles and forms a bed layer (cargo). The surplus of water in the hopper flows overboard through the overflow when the water level in the hopper exceeds the overflow level. Consequently, not settled sediment inside the hopper can flow overboard through this overflow discharge. Due to gravitational effects the fractions in the overflow discharge mainly contains the finer materials. Depending on the nature of in situ soil conditions (particle size distribution), the hopper geometry and other operational process parameters this overflow loss can be significant.

2.2 Existing hopper sedimentation models

Since the beginning of dredging activities with Trailing Suction Hopper Dredgers dredging contractors and researchers are interested in the physics of the sedimentation process inside the hopper. Consequently several sedimentation models are developed to describe this sedimentation process. These models primarily focusses on predictions of the amount of overflow losses during hopper filling.

One of the first models (Camp, 1946) originates from the sewage and water treatment industry and was developed to predict the settling rate of suspended particles. Suspended sediment transport was modelled by constant horizontal flow and constant vertical settlement of suspended particles. Based on the relative simple Camp model more sophisticated sedimentation models are developed. These models include more physical processes like vertical variation in settled bed level (Vlasblom & Miedema, 1995), hindered settling, sediment erosion (Miedema, 2008) or variation in vertical suspended sediment distribution (van Rhee, 2002), (Spearman, 2014).

A more sophisticated model is the 2DV flow model (van Rhee, 2002). This model is based on the (2D) Reynolds Averaged Navier Stokes equations and considers transport variation in the both the horizontal as the vertical. The 2DV model is validated against experimental model and prototype results. This model provides results for the overflow losses as well as a prediction of the bed level over the horizontal.

2.3 Limitations of the existing sedimentation models

Most of the existing sedimentation models provide reasonable accurate results for the total overflow losses. However the simplifications made in these models results in some limitations as described below:

- Except from the 2DV model (van Rhee, 2002) existing models consider only vertical flow variation (1DV) based on advection diffusion or they include simplified homogeneous (Spearman, 2014) or logarithmic horizontal flow. Hence, the influence of horizontal transport by density currents cannot be simulated within these models. Generation of density currents inside the hopper as a consequence of high density mixture discharge was already demonstrated (Koning , 1977) and quantified (van Rhee, 2002).
- The cross-sectional geometry of the hopper is not included in the existing models, geometry is simplified as a rectangular cross-sectional shape. Hence within these models the influence of the sloping hopper walls cannot be taken into account. This geometrical simplification can affect the flow and bed level evolution processes especially near the bottom of the hopper where cross-sectional variation can be significant.
- Longitudinal variation in bed level, water level as well as horizontal variation in velocity is not explicitly calculated in most models. Therefore, cargo distribution along the hopper length cannot be predicted within these models (except 2DV).
- Water and bed level cannot exceed the overflow level in most models. Especially when loading courser grains the bed level can exceed the overflow level at the inflow location.

- Drying and flooding of the sand bed as a consequence of lowering the overflow level cannot be modelled within these models.
- The position as well as the configuration of the inflow and overflow system is simplified in most models. Therefore it is difficult to predict the effect of different loading strategies within these models.

The shortcomings as mentioned above drive the initiative to develop a more process-based working tool which includes the relevant physical processes to predict the hopper sedimentation process.

2.4 Flow characteristics inside the hopper

The loading of a hopper is characterised by the inflow of high mixture densities concentrated at the loading position(s) of the hopper. The high density mixture acts like a buoyant jet flowing downwards towards the bottom to form high concentration sediment layers above the settled sediment bed, see Figure 2.2. The flow propagates horizontally as a density current over the settled sediment bed and is present during the whole loading process (Koning , 1977), (van Rhee, 2002).

The density current is characterised by higher concentrations with respect to the ambient water layer (van Rhee, 2002). This relative density difference with respect to the ambient water layer (buoyancy effect) is the driving force of the density current (Hallworth, 1996), (Bonnecaze, 1993). The density difference between the density current and the overlaying water layer changes continuously due to suspended sediment transport and sediment exchange with the bed.

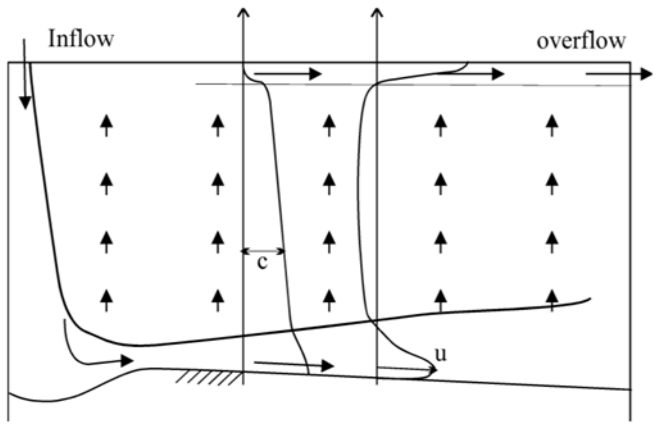

Figure 2.2: Schematisation of flow- and concentration pattern inside the hopper (van Rhee, 2002)

Figure 2.2 shows a schematic overview of the flow characteristics arising in the hopper during the loading phase as was already quantified by (van Rhee, 2002). Note the presence of the high density flow near the bed region. The downward plunging jet at the inflow forces an upward flowing water body over the entire length of the hopper. This vertical flow forces vertical transport of sediments. Sediment exchange between the bed interface caused by sediment settling and erosion results in longitudinal bed level variation.

Hence, a mathematical approach may be adopted which distinguishes the horizontal transport of suspended sediment into two vertically separate density layers which are dynamically coupled with the bed profile.

2.5 Conceptual model

Considering the summarised physical transport characteristics mentioned above together with the shortcomings of the existing models this gives rise to the development of a two-layered (1D) horizontal cross-section averaged model. A cross-section averaged approach is regarded to incorporate the cross-sectional hopper shape within a one-dimensional framework. Moreover, horizontal transport of water and sediment is divided into two separate density layers. The physical processes are proposed to be modelled with the following approach:

- The external (barotropic) water motion, is modelled with 1-D cross-section averaged shallow water equations.
- The effects of the internal (baroclinic) current are modelled with layer averaged baroclinic equations.
- Transport of suspended sediment in both currents is modelled with layer averaged advection equations.
- Settling of suspended sand causes sediment bed formation related to both erosion- and sedimentation expressions.
- Water motions, sediment transport and bed level evolution along the hopper length are derived in a one-dimensional cross-sectional averaged framework.
- Position as well as configuration of the inflow and overflow system can be specified.

2.6 Model Approach

Transport of water and sediment within this conceptualised model is divided into two separate layers, the external (barotropic) and internal (baroclinic) water motion, see Figure 2.3. Within these layers water and sediment is distributed horizontally by advection and mutual vertical transport is caused by settling, upward flow and entrainment processes. Sediment exchange with the bed interface results in settled bed variation and therefore the two hydrodynamic models are dynamically coupled to bed level variation.

Density (internal) current

The density current, also known as internal current, is modelled with vertically layer averaged velocities and concentrations (Bonnecaze, 1993), (Nijs, 2010) based on the shallow water equations. It is assumed that the internal flow do not affect the external flow dynamics based on the assumption that the total water depth is much larger compared to the internal layer depth $h<<H$. However, the external water layer forces the internal flow due to the external water level gradient.

Free surface (external) flow

The free surface (barotropic) water motion inside the hopper is characterised by lower suspended sediment concentration compared to the internal current especially at the beginning of the loading process. This free surface through flow is called external flow and is featured by a water depth to hopper length ratio which is much smaller than one, H<<L. This assumption implies the free surface water motion can be modelled based on the shallow water approach (Battjes & Labeur, 2014). Free surface (barotropic) flow is forced by a water surface gradient generated by the inflow/outflow discharge in the hopper. Water is extracted from this flow when the water level exceeds the overflow level.

The above mentioned two-layered horizontal suspended sediment transport model is shown in Figure 2.3.

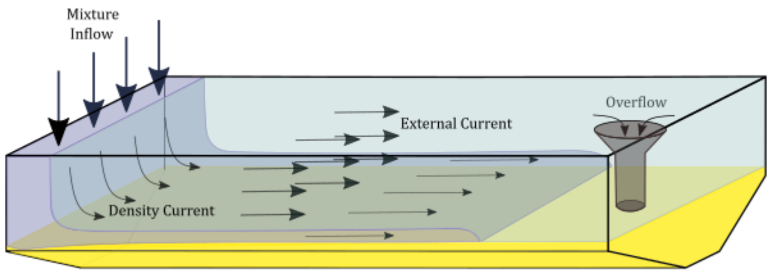

Figure 2.3: Schematisation of the cross-sectional averaged two-layered approach

Sediment exchange

The relatively high suspended sediment concentration present in the density current with respect to the ambient (external) water motion results in higher flow velocities (buoyancy effect) just above the settled bed region (van Rhee, 2002). These high flow velocities can cause sediment erosion which will be modelled with an expression for the pick-up flux. In addition, suspended sediment particles settle and form a bed layer.

Sediment exchange between the external and internal layer can arise as a consequence of the upward flow in the hopper, settling of sediment from external into internal and due to entrainment effects.

Cross-sectional averaged approach

To extend from existing models and to regard a more process-based approach the model includes the cross-sectional geometry of the hopper. Therefore, the most commonly used cross-sectional hopper shapes at trailing suction hopper dredgers can be specified, silo- and keelson hopper shape. The vertically converging hopper shape towards the bottom can considerably affects bed level evolution and flow characteristics.

3 Governing equations hopper sedimentation process

This chapter firstly elaborates the water and sediment transport due to the external (barotropic) water motion and secondly the contribution of the internal (baroclinic) water motion. Both the external as the internal water motions are derived based on the principle of one-dimensional cross-section averaged conservation of mass and momentum. The suspended sediment transport equations are derived analogous to the mass balances including specific terms related to the properties of sediment exchange such as settling and erosion. This results in a total set of six governing conservation equations. That is, two sets of three equations for both the internal and external water motion: continuity, suspended sediment conservation and momentum conservation. These equations yields values for the variables cross-sectional flow area, concentration and velocity.

3.1 The barotropic water motion and suspended sediment transport

The expression for the cross-section averaged external water motion is based on the 1-D shallow water equations for open channel flows (Battjes & Labeur, 2014). Here, to derive the external (barotropic) water motion and sediment transport a control volume is considered, see Figure 3.1, consisting of a cross-slice of the entire wet area.

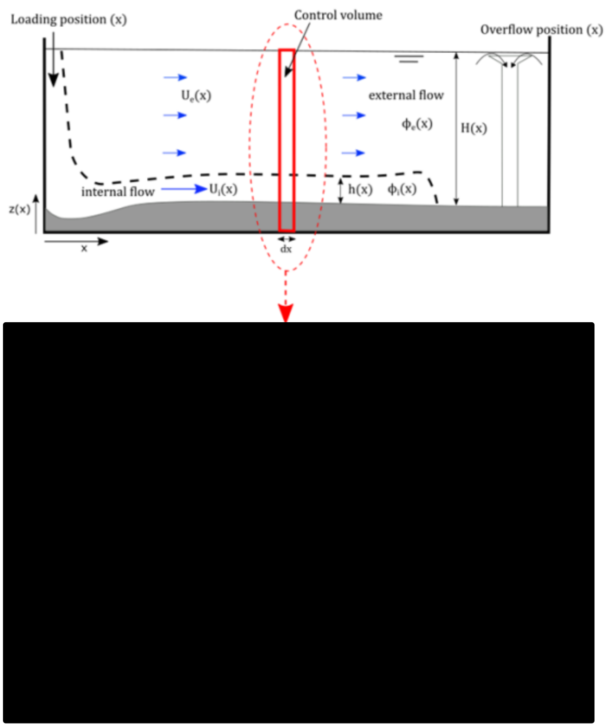

Figure 3.1: Schematisation of the mass balance describing the external water motion.

This control volume describes the total wet area from bed to free surface with length Δx. Cross-sectional averaged flow area variation within the control volume appears due to variation in cross-sectional hopper shape and water- and bed level variation in time.

3.1.1 Conservation of mass

The cross-section averaged mass conservation for the external water motion with contribution of additional source/sink terms and by considering incompressibility of the flow yields the continuity equation as presented in Figure 3.1. Note that horizontal velocity U is vertically uniform within the control volume following from the hydrostatic pressure assumption.

The expression as shown in Eq. 3.1 is obtained from continuity of mass after substitution of the assumption of incompressibility. Note that the flow area is variable in horizontal direction due to variation in water and bed level. This yields the expression for the continuity balance in terms of cross-section averaged flow area and vertically uniform flow velocity, with the contribution of inflowing and outflowing mass fluxes:

$$\frac{\partial \rho_m A_e}{\partial t} + \frac{\partial \rho_m A_e U_e}{\partial x} = P_{in,w,e} + P_{in,\phi,e} - P_{ov,w} - P_{ov,\phi} \tag{3.1}$$

The external layer density ρ_m is given as:

$$\rho_m = (1 - \phi_e)\rho_w + \phi_e \rho_s \tag{3.2}$$

Where A_e is the cross-section averaged external flow area, U_e is the vertically uniform flow velocity in the external layer (see Figure 3.1.), ρ_w is the density of water, ρ_s is the solids density of sand, t is time and x is a horizontal spatial distance. $P_{in,w,e}$ and $P_{in,\phi,e}$ are respectively the water- and sediment discharge (source) fluxes into the control volume, $P_{ov,w}$ and $P_{ov,\phi}$ are respectively the overflowing water- and sediment (sink) fluxes extracted from the control volume. Note that the inflowing/overflowing mass fluxes are only active at specified locations (inflow/overflow position).

Water- and sediment fluxes

Besides water and sediment inflow/overflow also sediment exchange between the bed and the overlaying currents are defined with flux expressions. This involves exchange between settled bed and the external current (without the presence of an internal current), between the bed interface and the internal current and between the internal and external current. This section describes the exchange flux expressions which affects the external conservation equations.

It is assumed water and sediment can enter or leave the whole (external) water column by the following physical processes:

- Water and sediment inflow at the loading location (in)
- Sediment Erosion (in)
- Sediment Deposition (out)
- Sediment Entrainment (in/out)

- Upward sediment flux (in)
- Water and sediment overflow at the overflow location (out)

The water and sediment fluxes describing exchange between the bed interface and the overlaying current(s) as mentioned above are shown in Figure 3.2.

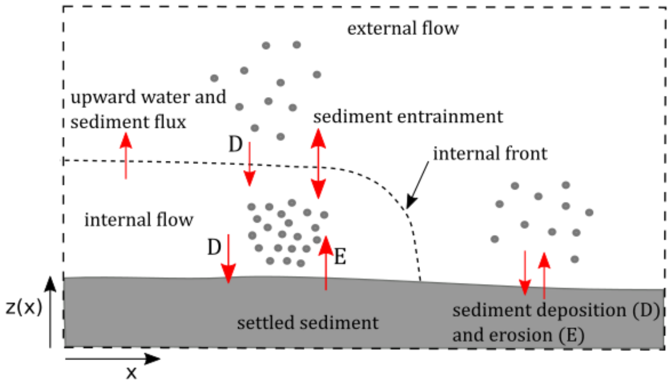

Figure 3.2 Sediment exchange fluxes

Mixture inflow

Hopper filling starts with the discharge of a water-sediment mixture into the hopper at the inlet location. Because the water and sediment balances are solved explicitly the discharge terms of water and sediment entering the hopper are treated separately (water and solids flux). Water discharge $P_{in;w,e}$ is given by:

$$P_{in;w,e} = \alpha\rho_w(1 - \phi_{inflow})\left(\frac{Q_{in}}{\Delta L_{in}B}\right) \tag{3.3}$$

Where ϕ_{inflow} is the inflow concentration into the hopper, Q_{in} is the discharge into the hopper, ρ_w is the water density, ΔL_{in} is the inflow length (number of cells) and α is a distribution factor to describe the amount of water entering either the internal or external layer. For given geometry of the cross-section, the width B may varies in time due to the changing water level inside the hopper. Therefore the width B varies in time in a known manner through the time variation of A_e, so the width of the layer at a certain location is defined as $B = B(x, A_e(x,t))$.

Sediment discharge $P_{in;\phi,e}$ into the control volume is given as:

$$P_{in;\phi,e} = \alpha\rho_s\phi_{inflow}\left(\frac{Q_{in}}{\Delta L_{in}B}\right) \tag{3.4}$$

Where ρ_s is the solids density of sand.

Mixture overflow

During the first phase of hopper filling the water level inside the hopper rises. When, after a certain time the water level reaches the overflow level a certain amount of mixture will flow overboard. This overflowing discharge can contain fractions of non-settled sediments. Therefore, the overflow discharge flux is separated into an overflowing water- and sediment flux which are presented below:

Overflowing water flux $P_{ov,w}$ is given as:

$$P_{ov,w} = \rho_w (1 - \phi_{ov}) \left(\frac{Q_{ov}}{\Delta L_{out} B} \right) \tag{3.5}$$

Where Q_{ov} is the overflow discharge, ϕ_{ov} is the concentration in the overflow mixture and ΔL_{out} is a specified length (number of cells) describing the overflow geometry.

The overflowing sediment flux $P_{ov,\phi}$ is given as:

$$P_{ov,\phi} = \rho_s \phi_{ov} \left(\frac{Q_{ov}}{\Delta L_{out} B} \right) \tag{3.6}$$

Sediment deposition

To reproduce the deposition of sediments a layer-averaged deposition flux is introduced based on the hindered settling velocity of particles. The sediment deposition flux in the external layer D_e is given as:

$$D_e = \rho_s \phi_e w_s \tag{3.7}$$

Where ϕ_e is the layer-averaged concentration in the external layer, w_s is the layer-averaged hindered settling velocity of grains with a certain diameter. For the full expression of the hindered settling velocity see section 4.2. The deposition flux is considered a balance between turbulent mixing effects and settling. In order to reproduce the near bed settling flux the deposition flux has to be corrected for the suspended sediment profile. Therefore the deposition flux can be chosen larger than the effective settling flux. The influence of this correction factor will be investigated in the numerical model simulations.

Erosion

The erosion rate is calculated with the expression for the pick-up flux (Van Rijn, 1993). Erosion of sediments occurs when the bed shear stress exceeds a certain threshold value. The pick-up flux is elaborated in section 4.1. Sediment erosion E is given by:

$$E = \phi_p \rho_s \sqrt{g \Delta d} \tag{3.8}$$

Where ϕ_p is the dimensionless pick-up flux (Van Rijn, 1993), see section 4.1, d is the particle diameter and Δ is the specific density.

Sediment entrainment flux

Due to the potential occurrence of flow velocity difference between the external and internal flow a sediment entrainment flux is introduced. Sediment entrainment is directed into the layer with the higher flow velocity (Pietrzak, 2015). The process of sediment entrainment $P_{E;\phi}$ is given here:

$$P_{E;\phi} = \rho_s \phi_k u_{ent} \tag{3.9}$$

Where ϕ_k can either be the internal or external concentration depending on the sign of the flux. The entrainment velocity u_{ent} depends on the flow velocity difference between the two layers. The expression for the entrainment velocity is explained in section 4.6.

Upward sediment flux
The mixture discharge at the loading position acts like a buoyant jet and as a consequence the discharged mixture propagates directly towards the bottom of the hopper. This downward propagating flow at the inflow location results in an upward flow (w) in the entire hopper as was already quantified by (van Rhee, 2002). The upward flow will result in vertical transport of water and sediment. Therefore a flux is introduced which transports water and sediment from the internal current into the external current. Upward sediment transport $P_{upw,\phi}$ is described with the following flux expression:

$$P_{upw,\phi} = \rho_s \phi_i (w - w_{s,i}) \tag{3.10}$$

Where w is the upward flow velocity present in the hopper and $w_{s,i}$ is the hindered settling velocity of a certain fraction of sediments. This means that the upward vertical transport of sediments is corrected with the downward hindered settling velocity for each fractions of sediments.

Bed level elevation
Sediment exchange between the bed interface results in vertical bed level variation within the control volume. The rate of bed mass change in time within the control volume contributes to the mass balance as presented below:

$$XXXXXXXXXXX = XXXXXXXXXXXXXXX \tag{3.11}$$

With $\Delta x \rightarrow 0$ the $O(\Delta x^2)$ term approaches zero much faster than first order term and hence can be neglected. This yields the following expression for the change in mass due to bed level variation:

$$\Rightarrow \rho_b \frac{\partial A_b}{\partial t} \Delta x \tag{3.12}$$

Where $\rho_b =$ bed density and A_b is the cross-sectional averaged bed area.

Mass conservation
With the contribution of the water- and sediment exchange processes and the additional bed level variation as described above conservation of mass can be derived for the external mixture. Adding the expression for the bed level elevation Eq.3.12 to Eq. 3.1 yields the external mixture balance as presented below:

$$\frac{\partial \rho_m A_e}{\partial t} + \frac{\partial \rho_m A_e U_e}{\partial x} = -XXX + XXX + XXX - XX + XX \tag{3.13}$$

Note that the width of the hopper B is variable in vertical direction when a non-square cross-sectional hopper shape is modelled. Hence the width B as described in the mass balance can either be width of the water level, width of the interface layer (interface between external and internal) or width of the bed interface. Therefore the width B is given as $B = B(x, A(x,t))$.

XXXXXXXXXXXXXXXXXXXXXXXXXXXXXXXXXXXXXXXXXXXXXXXXXXXXXXXXXXXXXXX XXXXXXXXXXXXXXXXXXXXXXXXXXXXXXXXXXXXXXXXXXXXXXXXXXXXXXXXXXXXXXX XXXXXXXXXXXXXXXXXX:

$$XX = XXXXXXXX \tag{3.14}$$

XXXXXXXXXXXXXXXXXXXXXXXXXXXXXXXXXXXXXXXXXXXXXXXXXXXXXXXXXXXXXXX XXXXXXXXXXXXXXXXXXXXXX:

$$XXXXXXXXXXXXXXXXXXXX = XXXXXXXXXXXXXXXXXX \tag{3.15}$$

XXXXXXXXXXXXXXXXXXXXXXXXXXXXXXXXXXXXXXXXXXXXXXXXX:

$$XXXXXXXXXX = \mathrm{XXXXXXXXXXXXXXXXXXXXXX} \tag{3.16}$$

XXXXXXXXXXXXXXXXXXXXXXXXXXXXXXXXXXXXXXXXXXXXXXXXXXXXXXXXXXXXXXX XXXXXXXXXXXXXXXXXXXXXXXXXXXXXXXXXXXXXXXXXXXXXXXXXXXXXXXXXXXXXXX XXXXXXXXXXXXXXXXXXXXXXXXXXXXXX.

3.1.2 Conservation of momentum

The dynamics of the external (barotropic) water motion are derived based on the one dimensional layer averaged shallow water equations. Within this 1D approach horizontal momentum is formulated in conservative form and is derived from a balance between inertia, external water gradient forcing and resistance.

The 1D cross-sectional averaged conservation of horizontal momentum is sketched within the control volume, as illustrated in Figure 3.3.

[redacted]

Figure 3.3: Control volume describing conservation of external momentum

The rate of change in momentum storage within the control volume is given as:

$$XXXXXXXXXXXXXXXXXX$$

$$= XXXXXXXXXXXXXXXXXXXX \tag{3.17}$$

The second order term is considered to approach naught much faster than the first order term at the limit $\Delta x \to 0$. This results in the expression for the rate of change in momentum storage within the control volume given as:

$$\Rightarrow \frac{\partial}{\partial t} \rho_m U_e A_e \Delta x \tag{3.18}$$

Inertia

Horizontal transport of momentum is derived from the net flux of horizontal momentum through the control volume boundaries. The net horizontal momentum flux across the control volume is derived as follows:

$$XXXXXXXXXXXXXXXXXXXXXXXXXXXXXXXXXXXXXX$$

$$= XXXXXXXXXXXXXXXXXXXXXXXXXXXXXXXXXXXX \tag{3.19}$$

XXXXXXXXXXXXXXXXXXXXXXXXXXXXXXXXXXXXXXXXXXXXXXXXXXXXXXXXXXXXXXXXXXXX XXXXXXXXXXXXXXX:

$$\Rightarrow \frac{\partial \rho_m U_e^2 A_e}{\partial x} \Delta x \tag{3.20}$$

Hydrostatic pressure force

A horizontal water surface gradient (due to mixture inflow/overflow) causes the existence of an external hydrostatic pressure term. The water level gradient forces the external water layer to flow from the discharge location towards the overflow location. The forcing as a result of the slope of the free surface is derived as follows:

$$XXXXXXXXXXXXXXXXXX =$$

$$= XXXXXX \tag{3.21}$$

This yields the expression for the pressure forcing $F_{p,e}$ as presented below:

$$F_{p,e} = -\rho_m g \left(A_e \frac{\partial H}{\partial x} \Delta x \right) \tag{3.22}$$

Where H is the total depth of the external flow.

Flow resistance

The resistance experienced by the water flow over the settled sediment bed profile is expressed as (Battjes & Labeur, 2014):

$$\Delta W = \tau_b P \Delta x \tag{3.23}$$

Where P is the length of the wetted perimeter and the bed shear stress τ_b is a non-linear term expressed as:

$$\tau_b = c_f \rho_m |U_e| U_e \tag{3.24}$$

Where c_f is a dimensionless friction coefficient. This results in the flow resistance expression F_r for the external flow as presented below:

$$F_r = c_f \rho_m |U_e| U_e P \Delta x \tag{3.25}$$

Bed slope

A mass on a sloping bed surface is subjected to a downslope reaction force caused by gravity. This gravity force term F_g is defined as follows:

$$F_g = (sin\theta) g M \tag{3.26}$$

Where M is the total water-sediment mass within the control volume. The bed slope is defined as the bed gradient, $\sin(\theta) = \frac{\partial z}{\partial x}$, substitution of these expressions yields:

$$\Rightarrow XXXXXXXXXXXXXXXXXXXXXX \tag{3.27}$$

XXXXXXXXXXXXXXXXXXXXXXXXXXXXXXXXXXXXXXXXXXXXXXXXXXXXXXXXXXXXXXXXXXXXXXXXX XXXXXXXXXXXXXXXXXXXXXXXXXXXXXXXXXXXXXXXXXXXXX:

$$F_g = \rho_m g A_e \frac{\partial z}{\partial x} \Delta x \tag{3.28}$$

Momentum conservation

The external momentum equation in conservative form follows from a balance between inertia, pressure force, bed slope and flow resistance terms as presented above. By considering a constant spatial step (Δx) this yields:

$$XXXXXXXXXXXXXXXXXXXXXXXXXXXXXXXXXXXXXXX = 0 \tag{3.29}$$

By assuming incompressibility of the mixture flow and by substituting the expression for the flow height $H = \xi_e - z$ this yields the conservative momentum balance as presented below:

$$XXXXXXXXXXXXXXXXXXXXXXXXXXXXXXXXXX = 0 \tag{3.30}$$

The formulation for the acceleration equation as presented in Eq. 3.30 is similar to the one-dimensional Saint-Venant equations.

3.1.3 Conservation of suspended sediment

Discharge of water and sediment into the hopper causes external water surface gradients generating currents that transport suspended sediment horizontally. Vertical transport of suspended sediment is not explicitly calculated within this model and therefore modelled with additional flux expressions as described in section 3.1.1. In this paragraph horizontal layer-averaged transport of sediment in the external water layer is derived based on the 1D horizontal advection equation.

Suspended sediment conservation

Conservation of suspended sediment within the control volume is obtained from a balance between horizontal transport by advection and vertical sediment exchange fluxes, as shown in Figure 3.4. Here two different flow situations are considered which can develop inside the control volume, the presence of an internal layer or no internal layer. Note the difference between the sediment exchange fluxes for these two cases.

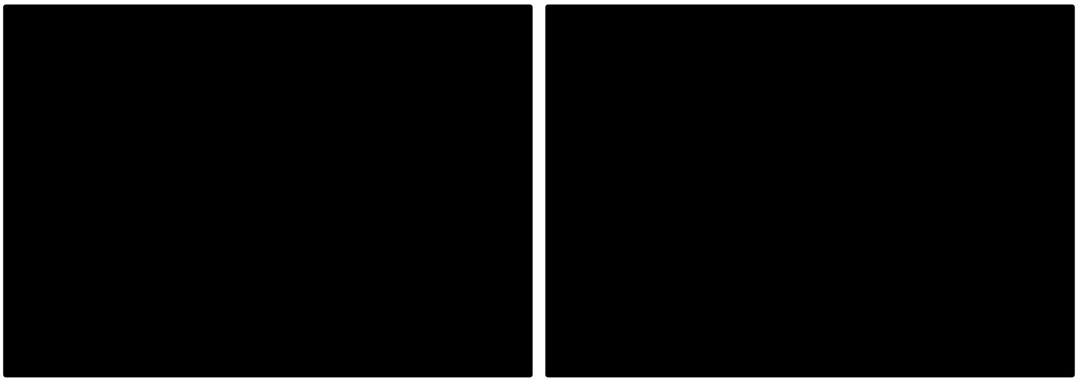

Figure 3.4: Left figure shows the sediment balance when no internal flow is present. Right figure shows the sediment balance with the presence of an internal current.

Here the layer-averaged horizontal advection equation without additional sediment source/sink terms is given in conservative form:

$$\frac{\partial \phi_e A_e}{\partial t} + \frac{\partial \phi_e A_e U_e}{\partial x} = 0 \tag{3.31}$$

Sediment source/sink terms

As illustrated in the control volume in Figure 3.4 and as already mentioned in section 3.1.1 multiple sediment exchange processes affects the sediment concentration in the external layer. To yield conservation of sediments (mass) these additional exchange fluxes are included in the horizontal advection balance (Eq. 3.31). Note that some of these exchange fluxes are only active with the presence of an internal current or at the inflow or overflow location.

Hence, when no internal flow is present, the external sediment deposition flux is directly into the bed. However with the presence of an internal layer the external deposition flux enters the internal layer. Subsequently the erosion flux can either enter the internal current or the bed layer depending on the presence of the internal layer. Note that the velocities in the external layer are very low during almost the whole loading process and therefore erosion due to this current is not likely to occur.

Sediment conservation

Including the sediment source/sink fluxes as described in section 3.1.1 into the horizontal advection equation (Eq. 3.31) yields the cross-section averaged suspended sediment balance in conservative form as presented below:

$$\boxed{\frac{\partial \phi_e A_e}{\partial t} + \frac{\partial \phi_e A_e U_e}{\partial x} = XXXX + XXXX + XXX + XXXX - XXXXX} \tag{3.32}$$

With the derivation of the suspended sediment balance in conservative form as presented in Eq. 3.32 a solvable equation for the water balance (Eq. 3.16) can be derived. To get a solvable water balance the sediment balance (Eq. 3.32) is substituted in Eq. 3.16 which yields:

$$\boxed{\frac{\partial A_e}{\partial t} + \frac{\partial A_e U_e}{\partial x} = XXX + XXX + XXX - X(XX + (X - X)X - XX) - XX - XX} \tag{3.33}$$

3.2 The baroclinic water motion and suspended sediment transport

The internal current arising from high concentration flows concentrated near the bed is modelled with layer-averaged baroclinic equations (Pantin, 1979), (Bonnecaze, 1993), (Nijs, 2010) and here in a conservative form (Nijs, 2010). This approach includes one-dimensional layer averaged formulations for turbidity currents and sediment transport. The water motion and suspended sediment transport for the internal current are fully represented by the conservation equations for the water-sediment mixture, the sediment in the current and the momentum in horizontal direction.

System of conservation equations

The derivation of the system of conservation equations describing the internal current is analogous to the derivation of the external current as derived in Chapter 3.1. The most important difference with respect to the external layer water motion is the contribution of a density gradient forcing (buoyancy effect) and the presence of the ambient (external) water layer.

In this section the basic principles of the derivation and the final formulations for the density driven water balance, sediment balance and momentum balance are presented. For derivation of the density driven (baroclinic) water motion and sediment transport a control volume is considered, see Figure 3.5, consisting of a cross-slice of the internal wet area. This control volume describes the wet area from bed to interface between the two layers with length Δx.

3.2.1 Conservation of suspended sediment

Layer-averaged horizontal sediment transport is described by the horizontal (1D) advection equation as is shown in Figure 3.5 and presented below:

$$\frac{\partial \phi_i A_i}{\partial t} + \frac{\partial \phi_i U_i A_i}{\partial x} = XXXXXXXXXXXX \tag{3.34}$$

[redacted]

Figure 3.5: Control volume describing the internal sediment balance

Where A_i is the cross-sectional internal flow area, U_i is the internal flow velocity and ϕ_i is the layer-averaged suspended sediment concentration within the internal layer.

Sediment source/sink terms

Suspended sediment fluxes in the internal current arises from sediment exchange between the bed interface (erosion and deposition) and between the ambient current due to sediment deposition, entrainment and vertical flow induced sediment exchange processes. These sediment exchange fluxes are described in section 3.1.1.

Water sediment discharge entering the hopper causes sediment inflow at the loading position. Because the model is vertically divided into two layers, the mixture can either flow into the external layer or into the internal layer. Therefore a distribution factor α is introduced which determines the amount of inflow in each layer.

Sediment discharge into the internal layer $P_{in;\phi,i}$ is given as:

$$P_{in;\phi,i} = (1-\alpha)\rho_s \phi_{inflow}\left(\frac{Q_{in}}{\Delta L_{in} B}\right) \tag{3.35}$$

Due to the buoyancy effect it is assumed that the total inflowing mixture directly flows towards the bed and forms a density current, this effectively means $\alpha = 0$.

Mass conservation for sediment

Including the sediment exchange fluxes into the (1D) cross-section averaged advection equation yields the sediment balance for suspended sediments in the internal current in conservative form as presented below:

$$\boxed{\frac{\partial \phi_i A_i}{\partial t} + \frac{\partial \phi_i U_i A_i}{\partial x} = XX + XX + XX - XX - XX} \tag{3.36}$$

3.2.2 Conservation of mass

The continuity equation for the internal current is derived analogue to the derivation of the external continuity equation. Figure 3.6 shows the control volume describing the internal mass balance.

[redacted]

Figure 3.6: Control volume describing the internal mass balance

The mixture balance with additional sediment and water inflowing fluxes follows from continuity as derived in Eq. 3.1 and is presented below for the internal current:

$$\frac{\partial \rho_m A_i}{\partial t} + \frac{\partial \rho_m A_i U_i}{\partial x} = XX + XX \tag{3.37}$$

Note that the mixture density for both the external as well as the internal current is explicitly calculated by the sediment balance for these particular layers.

Water and sediment fluxes

The water and sediment exchange fluxes describing the inflow of water and sediments, erosion, settling, entrainment and vertical sediment transport are elaborated in section 3.1.1.

Bed level elevation

Sediment exchange between the bed results in vertical bed level variation within the control volume. Variation in bed level within the control volume contributes to the mass balance analogues as in the external current, section 3.1.1, and is shown below:

$$\Rightarrow \rho_b \frac{\partial A_b}{\partial t} \Delta x \tag{3.38}$$

Conservation of mass

To get a solvable water balance the expression for the mixture density is reformulated and substituted in the sediment balance as presented below. The internal mixture density is expressed in terms of layer-averaged internal concentration, density of water and density of solids as:

$$\rho_m = (\phi_i \Delta + 1)\rho_w \tag{3.39}$$

Substitution of the reformulated mixture density term Eq. 3.40, in Eq. 3.38 and by including the bed level elevation rate (Eq. 3.39) yields the mixture balance as presented below:

$$XXX + XXX = XXX + XXX + XXX \tag{3.40}$$

Specific density and water density considered as constants results in:

$$XX + XX + XXX = XXX + XX \tag{3.41}$$

XXXXXXXXXXXXXXXXXXXXXXXXXXXXXXXXXXXXXXXXXXXXXXXXXXXXXXXXXXXXXXXXXXXXXXXXXXXXXXXXXXXXXXXX XXXXXXXXXXXXXXXXXXXXXX as expressed in Eq. 3.36. Substitution of Eq. 3.36 in Eq. 3.41 yields the water-sediment balance in conservative form as presented below:

$$\boxed{\frac{\partial A_i}{\partial t} + \frac{\partial A_i U_i}{\partial x} = XXXXXXXXXXXXXXXXXXXXXXXXXXXXXXXXX} \tag{3.42}$$

3.2.3 Conservation of internal momentum

The internal water motion is fully described by conservation of internal momentum. Here it is formulated in conservative form and consists of a balance between inertia, pressure forcing (internal and external), bed slope and resistance, see Figure 3.7.

[redacted]

Figure 3.7: Control volume expressing internal momentum balance

XXXXXXXXXXXXXXXXXXXXXXXXXXXXXXXXXXXXXXXXXXXXXXXXXXXXXXXXXXXXXXXXXXXXXXXX XXXXXXXXXXXXXXXXXXXXXXXXXXXX. The difference compared with the external momentum equation is the additional contributions of the relative density gradient and the influence of the ambient water layer on the internal current (external pressure). This section describes the derivation of each term in the momentum equation. XXXXXXXXXXXXXXXXXXXXXXXXXXXXXXXXXXXXXXXXXXXXXXXXXXXXXXXXXXXXXXXXXXXX.

Rate of change in momentum storage

$$XXXXXXXXXXXXXXXXXXXXXX =$$

$$\Rightarrow XXXXXXXXXXXXX \tag{3.43}$$

Net Horizontal momentum flux

$$XXXXXXXXXXXXXXXXXXXXXXXXXXXXXXXXXXXXX =$$

$$\Rightarrow XXXXXXXXXXXXXXX \tag{3.44}$$

Hydrostatic pressure force

The hydrostatic pressure gradient in the internal layer causes a horizontal pressure forcing $F_{p,i}$ derived as follows:

$$XXXXXXXXXXXXXXXXXXXX =$$

$$\Rightarrow \frac{\partial F_{p,i}}{\partial x} \Delta x \tag{3.45}$$

Substituting the internal pressure expression, Eq. 3.44 in Eq. 3.44 yields:

$$XX = XXX + XXXX \tag{3.46}$$

Where ρ_e and ρ_i are respectively the external and internal layer density and h is the internal layer height. Note the additional term following from the contribution of the external hydrostatic pressure gradient.

Hence, the pressure forcing in the internal current consists of an density difference term (buoyancy effect) and forcing due to the external water surface gradient. The water surface gradient pressure forcing is rewritten with $H = \xi - z$. This yields an internal pressure forcing as presented below:

$$XX = XXXX + XXXXX \tag{3.47}$$

Bed slope

A longitudinal bed gradient causes a downslope reaction force due to gravity. Assume contribution of the internal mass (reduced density) and the mass of the external layer for calculating the total mass on the slope. The internal gravity force F_g on a sloping bed yields:

$$F_g = Mg \cdot sin(\theta) = Mg\frac{\partial z}{\partial x}$$

$$X = XXXX + XXXXXX \tag{3.48}$$

XXXXXXXXXXXXXXXXXXXXXXXXXXXXXXXXXXXXXXXXXXXXXXXXXXXXXXXXXXXXXXXXXXXXXXXX XXXXXXXXXXXXXXXXXXXXXXXXXXXXXXXXXXXXXXXXXXXXXXXXXXXXXXXXXXXXXXXXXXXXXXXX XXXXXXXXXXXXXXXXXXXXXXXXXXXXXXXXXXXXXX:

$$XX = XXXXX + XXXXX \tag{3.49}$$

$$X = XXXXXXXXXXX \tag{3.50}$$

Internal flow resistance

Internal flow resistance is assumed to be a combination of bed shear stress (τ_b) and interface stress (τ_i). The interface stress is caused by a velocity difference between the external and internal flow. Hence the total flow resistance is defined by a combination of the bed shear stress τ_b and an interface shear stress τ_i. Therefore, the contribution of the internal flow resistance is expressed as follows:

$$\Rightarrow \tau_b B_b \Delta x + \frac{U}{\sqrt{U^2}} \cdot \tau_i B_i \Delta x \tag{3.51}$$

Where τ_b is the bed shear stress, τ_i is the interface stress, B_b is the width of the bed interface and B_i is the width of the interface between the external and internal layer.

Momentum balance
XX:

$$XXXXXXXXXXXXXXXXXXXXXXXX = XXXXXXXXXXXXXXXXXX$$

XXXXXXXXXXXXXXXXXXXXXXXXXXXXXXXXXXXXXXXXXXXXXXXXXXXXXXXXXXXXXXXXXXXXXXXXXXXXXXXXXXXXXXXXXXXXXXXXXXXXXXXXXXXXXXXXXXXXXXXXXXXXXXXXXXXXXXXXXXXXXXXXXXXXXXXXXXXXXXXXXXXXXXXX:

$$\boxed{XX + XXX + XXXX + XXX + XXX = XXX + XXXX} \qquad (3.52)$$

XXXXXXXXXXXXXXXXXXXXXXXXXXXXXXXXXXXXXXXXXXX

3.3 Bed level evolution rate

Sediment exchange between the settled bed interface and the ambient water-sediment layer causes longitudinal and vertical bed level variations. The rate of bed level elevation in time is determined by erosion and sedimentation processes (van Rhee, 2002). Within this mathematical framework bed level elevation is expressed as variation in cross-section averaged bed area.

Conservation of mass

Cross-section averaged bed level elevation is derived from the conservation of mass between the bed interface. The sediment erosion and deposition fluxes can cause a horizontal bed level gradient along the hopper. The prediction of longitudinal variation in bed level is one of the main objectives of this model. Figure 3.8 shows a schematisation of the cross-section averaged approach describing bed level variation.

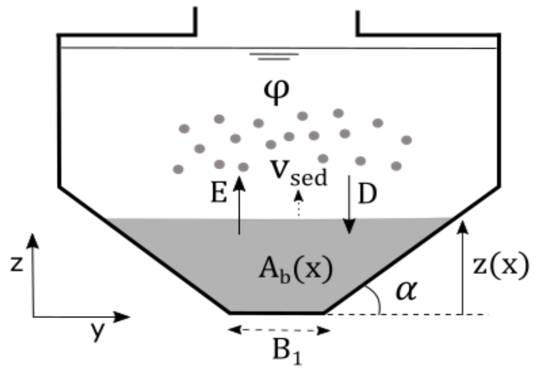

Figure 3.8: Cross-sectional sketch bed area elevation

Conservation of mass is derived from exchange fluxes between the bed interface as presented below:

$$change\ in\ stored\ mass: \quad XXXXXXXXXXXXXXXXXXXXXXX$$

$$\Rightarrow XXXXXXXXXXXXXXXXXXXXXXXXX \tag{3.53}$$

Where n_0 = bed porosity and z is a vertical spatial distance. Change in bed interface width in longitudinal direction within the control volume is considered constant for small spatial steps, with this assumption the change in stored mass yields:

$$\Rightarrow XXXXXXXXXXXXXXXX \tag{3.54}$$

The net vertical mass flux between the bed interface yields:

$$XXXXXXXXXXXXXXXXXXXXXXX \tag{3.55}$$

Where the additional term $\phi \frac{\partial z}{\partial t}$ arises from the bed level elevation rate. The upward moving bed interface causes an increase in sediment settling as was shown by (van Rhee, 2002).

The near bed concentration ϕ can either be the internal or external concentration depending on the presence of an internal flow. Variation in bed level elevation in time $\frac{\partial z}{\partial t}$ is known as the bed level elevation rate.

A balance between the stored mass (Eq.3.54) and the net mass flux (Eq.3.55) between the bed interface yields the mass balance as presented below:

$$\Rightarrow (1 - n_0)\frac{\partial A_b}{\partial t} = XXXXXXXXXXXXXXXXXXXXXXXXX$$

$$\frac{\partial A_b}{\partial t} = XXXXXXXXXXXXXXXXX \tag{3.56}$$

Where A_b is the cross-sectional bed area, the bed interface width variation is a known function of the cross-sectional geometry of the hopper.

For a square cross-section (constant width B, $\frac{\partial B}{\partial z} = 0$) the expression for bed level elevation yields:

$$\frac{\partial z}{\partial t} = \frac{(D - E)}{(1 - n_0 - \phi)} \tag{3.57}$$

3.4 Total set of equations

The external and internal water motion and suspended sediment transport are fully described by the total set of six conservation equations as derived in the previous sections. Here the governing one-dimensional cross-section averaged equations are summarised in conservative form. From these governing equations the variables describing the external and internal flow area, sediment concentration and velocity can be derived.

Cross-sectional bed area variation:

$$XX = XXXX \tag{3.58}$$

External water motion and suspended sediment transport:

$$\begin{aligned} &XX + XX = -XX + XX + XX - XX - XX - XX \\ &XX + XX = XX + XX + XX + XX - XX \\ &XX + XX + XX + XX = 0 \end{aligned} \tag{3.59}$$

Internal water motion and suspended sediment transport:

$$\begin{aligned} &XX + XX = -XX - XX + XX + XX \\ &XX + XX = XX + XX + XX - XX - XX \\ &XX + XX + XX + XX + XX = XX + XXX \end{aligned} \tag{3.60}$$

4 Closure relations

In this section a set of auxiliary expressions are introduced to close the set of equations summarised in section 3.4.

4.1 Erosion

Settled sediment erodes from the bed layer when the bed shear stress exceeds a certain threshold value. The erosion rate caused by the overlaying current is derived based on an expression for the pick-up flux (Van Rijn, 1993). Note that the internal current is the main initiator of erosion due to the higher flow velocities in the internal current.
In this section the expression for the pick-up flux is elaborated. The method (Van Rijn, 1993) is based on low flow velocities up to 1.0 m/s.

Van Rijn's pick up flux
The pick-up flux (Van Rijn, 1993) estimates the erosion behaviour of single particles for flow velocities of 0.5-1.0 [m/s]. The Van Rijn expression overestimates the pick-up flux at higher flow velocities (>1.0 m/s).

The pick-up flux E is described with the following relation:

$$E \ = \phi_p \rho_s \sqrt{g \Delta d} \tag{4.1}$$

Where ϕ_p is the dimensionless pick-up flux, d is the particle diameter and Δ is the specific density.

The empirical formulation for the dimensionless pick-up flux for flow velocities in the range of 0.5 to 1.0 m/s yields (Van Rijn, 1993):

$$\phi_p = 0.00033 D_*^{0.3} \left(\frac{\theta - \theta_{cr}}{\theta_{cr}}\right)^{1.5} \tag{4.2}$$

Where θ is the shields parameter, θ_{cr} is the critical shields parameter and D_* is the dimensionless particle diameter:

$$D_* = d \left(\frac{\Delta g}{\nu^2}\right)^{1/3} \tag{4.3}$$

Particles are picked up by the flow when the actual shear stress exceeds the critical value, so when the Shields parameter (θ) exceeds the critical Shields parameter (θ_{cr}). The Shields parameter is calculated with the layer averaged flow velocity as follows:

$$\theta = \frac{f_0 U^2}{8 \Delta g d} \tag{4.4}$$

Where the friction factor f_0 for sand has a value of 0.02, U is the layer averaged flow velocity of the overlaying current.

The critical shields parameter is determined with the expression of (Brownlie, 1981):

$$\theta_{cr} = 0.22R_p^{-0.6} + 0.06\exp(-17.77 \cdot R_p^{-0.6}) \tag{4.5}$$

Where the particle Reynolds number (R_p) is calculated as follows:

$$R_p = \frac{d\sqrt{\Delta gd}}{\nu} \tag{4.6}$$

Where ν is the kinematic viscosity of the fluid.

Hence, when the shields parameter exceeds the critical shields parameter particles are picked up (E) by the overlaying current. Therefore, if $E > D$ net erosion takes place and the bed level decreases.

4.2 Sediment Deposition

Settling of suspended sediment from the overlaying water-sediment layer into the bed interface is determined by the concentration and soil characteristics of the suspended sediment in the ambient layer. High concentrations negatively influence the settling behaviour of single particles (van Rhee, 2002). This hindered settling behaviour is covered by the expression for the hindered settling velocity derived by (Richardson, 1954). The sediment deposition flux D is obtained by the product of hindered settling velocity and near bed concentration:

$$D = w_{s,i}\phi_i\rho_s \tag{4.7}$$

Where $w_{s,i}$ is the hindered settling velocity of a certain fraction (i),ϕ_i is the ambient layer-averaged concentration of fraction i. Note that the concentration in the deposition flux is given by the layer averaged concentration instead of the near-bed concentration. Therefore, the deposition flux may be corrected to incorporate the influence of the near bed concentration. This effect is shown in section 7.2.

The hindered settling velocity of sand due to high sediment concentrations (Richardson, 1954) reads:

$$w_s = w_0(1-c)^n \tag{4.8}$$

Where w_0 is the unhindered settling velocity of a single grain and c is the suspended sediment concentration.

The expression for the settling velocity w_0 of a single particle is expressed as (Ferguson & Church, 2004):

$$w_0 = \frac{\Delta gd^2}{C_1\nu + \sqrt{0.75C_2\Delta gd^3}} \tag{4.9}$$

Where the constants C_1 = 18 and C_2 = 1 for natural sand, d is the sediment particle diameter and ν is the kinematic viscosity of the surrounded water.

A way to compute the power n is from the empirical expression derived by (Rowe, 1987):

$$n = \frac{4.7 + 0.41 R_{e\,p}^{0.75}}{1 + 0.175 R_{e\,p}^{0.75}} \tag{4.10}$$

Where the particles Reynolds number is based on the settling velocity of a single particle and is defined as:

$$Re_p = \frac{w_0 d}{\nu} \tag{4.11}$$

4.3 Influence of particle size distribution

The expression for the hindered settling velocity as given in previous paragraph only holds for mono-sized particles. Natural sands consists of multiple particle sizes. To incorporate the poly disperse suspension another approach has to be applied. Because large particles settles faster than small particles there will be a mutually influence between the different graded particles. The counter flow created by settling of the particles influences the settling velocity of the particles.

The particle size distribution is calculated by a certain number N of different particle sizes with a certain concentration c_i. The counter flow generated by settling of grains results in a slip velocity relative to the upward fluid velocity. According to (Mirza & Richardson, 1979) an expression for the slip velocity v_s of a certain fraction i reads:

$$v_{s,i} = w_{0,i}(1 - c_t)^{n_i - 1} \tag{4.12}$$

Where c_t is the total volumetric concentration, $w_{0,i}$ is the settling velocity of fraction i and n_i is the hindered settling exponent of fraction i.

The upward velocity due to the combined settling of all fractions is derived from the control volume balance in vertical direction. The total volume displaced due to vertical settling is zero hence:

$$\sum_{j=1}^{N} c_j w_{s,j} + \left(1 - \sum_{j=1}^{N} c_j\right) v_w = 0 \tag{4.13}$$

Where v_w is the vertical upward water velocity. The first term in Eq. 4.13 expresses the combined settling of all fractions.

The settling velocity of one fraction $w_{s,i}$ is the sum of the water velocity and the slip velocity of that fraction:

$$w_{s,i} = v_w + v_{s,i} \tag{4.14}$$

Substitution of this expression into Eq. 4.13 and by rewriting this can be simplified to:

$$v_w = -\sum_{j=1}^{N} c_j v_{s,j} \tag{4.15}$$

Substitution of this formulation into Eq. 4.14 yields the vertical settling velocity of a certain fraction:

$$w_{s,i} = v_{s,i} - \sum_{j=1}^{N} c_j v_{s,j} \tag{4.16}$$

4.4 Water/sediment inflow conditions

The water and sediment discharge enters the hopper at the inlet location(s). This mixture discharge entering the hopper behaves as a buoyant jet. Most of the inflowing sediment mixture moves towards the hopper bottom where it forms a density current which propagates horizontally (van Rhee, 2002). When the total discharged mixture immediately forms a density current towards the bottom no sediment enters the external layer. This means no sediment leaves the buoyant jet before it reaches the bottom.

Because the mixture discharge into the hopper behaves like a buoyant jet, water and sediment entrainment into this fast flowing jet could occur (van Rhee, 2002). However this process is not included within this model approach. The flux expressions describing the water and sediment discharge into either the internal or external layer are described below:

Sediment discharge flux entering external flow :

$$P_{in;\phi,e} = \alpha \rho_s \phi_{inflow} \left(\frac{Q_{in}}{\Delta L_{in} B} \right) \tag{4.17}$$

Sediment discharge flux entering internal flow:

$$P_{in;\phi,i} = (1-\alpha) \rho_s \phi_{inflow} \left(\frac{Q_{in}}{\Delta L_{in} B} \right) \tag{4.18}$$

Where α is the distribution factor of water/sediment entering either the external or internal layer and ϕ_{inflow} is the inflowing concentration into the hopper.
Water discharge entering external flow:

$$P_{lp;w,e} = \alpha \rho_w (1 - \phi_{inflow}) \left(\frac{Q_{in}}{\Delta L_{in} B} \right) \tag{4.19}$$

Water discharge entering internal flow:

$$P_{lp;w,i} = (1-\alpha) \rho_w (1 - \phi_{inflow}) \left(\frac{Q_{in}}{\Delta L_{in} B} \right) \tag{4.20}$$

4.5 Water/sediment outflow conditions

When the water level inside the hopper exceeds the overflow level water and suspended sediment flow back overboard. This outflow is also known as overflow loss or production. Finally overflow losses are decisive for the total loading efficiency of the hopper. Because the courser material settles more easily with respect to finer material and forms either a bed- or an internal suspension layer the overflowing mixture contains the finer material. Here the overflow discharge is determined with two different principles: free overflow and submerged overflow (Battjes & Labeur, 2014).

XXXXXXXXXXXXXXXXXXXXXXXXXXXXXXXXXXXXXXXXXXXXXXXXXXXXXXXXXXXXXXXXXXXXX XXXXXXXXXXXXXXXXXXXXXXXXXXXXXXXXXXXXXXXXXXXXXXXXXXXXXXXXXXXXXXXXXXXXX XXXXXXXXXXXXXXXXXXXXXXXXXXXXXXXXXXXXXXXXXXXXXXXXXXXXXXXXXXXXXXXXXXXXX XXXXXXXXXXXXXXXXXX:

Free overflow:

$$XX = XXXXXXXXXXXX \tag{4.21}$$

$$XX = XXXXXX + XX \tag{4.22}$$

XXXXXXXXXXXXXXXXXXXXXXXXXXXXXXXXXXXXXXXXXXXXXXXXXXXXXXXXXXXXXXXXXXXXX XXXXXXXXXXXXXXXXXXXXXXXXXXXXXXXXXXXXXXXXXXXXXXXXXXXX.

Submerged overflow:

$$XX = XXXXXXXXXXXXXX \tag{4.23}$$

XXXXXXXXXXXXXXXXXXXXXXXXXXXXXXXXXXXXXXXXXXXXXXXXXXXXXXXXXXXXXXXXXXXXX XXXXXXXXXXXXXXXXXXXXXXXXXXXXXXXXXXXXXXXXXXXXXXXXXXXXXXXXXXXXXXXXXXXXX XXXXXXXXXXXXXXXXXXXXXXXXXXXXXX. In this approach the overflow losses are a function of the cross-sectional averaged concentration and velocity in the upper layer. This effectively means that the concentration and velocity derived in the external layer determines the overflow losses.

4.6 Sediment entrainment between layers

Sediment entrainment between the external and internal layer as a consequence of turbulent fluctuations is described with the velocity difference between the two currents. The direction of the entrainment depends on the magnitude of the flow velocities, this means entrainment is directed into the layer with the higher flow velocity (Pietrzak, 2015). Because vertical velocity gradients are not considered within this hydrodynamic model the vertical sediment transport due to turbulence fluctuations is modelled as a sediment source term as follows:

$$XX = XX = XXXXXX \tag{6.24}$$

Where the subscript k refers to either the internal or external layer, the horizontal velocity difference between the layers $\Delta U = U_i - U_e$, ϕ_k is either the internal or external concentration depending on the sign of the entrainment flux and α is a factor to determine the magnitude of the entrainment flux.

4.7 XXXXXXXXXXXXXXXXXXXXX

XXXXXXXXXXXXXXXXXXXXXXXXXXXXXXXXXXXXXXXXXXXXXXXXXXXXXXXXXXXXXXXXXXXXXXXXX XXXXXXXXXXXXXXXXXXXXXXXXXXXXXXXXXXXXXXXXXXXXXXXXXXXXXXXXXXXXXXXXXXXXXXXXX XXXXXXXXXXXXXXXXXXXXXXXXXXXXXXXXXXXXXXXXXXXXXXXXXXXXXXXXXXXXXXXXXXXXXXXXX XXXXXXXXXXXXXXXXXXXXXXXXXXXXXXXXXXXXXXXXXXXXXXXXXXXXXXXXXXXXXXXXXXXXXXXXX XXXXXXXXXXXXXXXXXXXXXXX:

$$X = \frac{X}{X} \tag{6.25}$$

XXXXXXXXXXXXXXXXXXXXXXXXXXXXXXXXXXXXXXXXXXXXXXXXXXXXXXXXXXXXXXXXXXXXXXXXX XXXXXXXXXXXXXXXXXXXXXXXXXXXXXXXXXXXXXXXXXXXXXXXXXXXXXXXXXXXXXXXXXXXXXXXXX XXXXXXXXXXXXXXXXXXXXXXXXXXXXXXXXXXXXXXXXXXXXXXXXXX:

$$XX = XX = XXXXX \tag{6.26}$$

XXXXXXXXXXXXXXXXXXXXXXXXXXXXXXXXXXXXXXXXXXXXXXXXXXXXXXXXXXXXXXXXXXXXXXX.

5 Numerical Implementation

5.1 Numerical method

The governing cross-sectional (1D) conservation equations describing the external and internal flow forms a hyperbolic system of equations. This system is solved on a staggered grid with a Finite Volume approach to ensure conservation. This approach is proven to be an accurate method for discretization of the shallow water equation (Stelling , Kernkamp, & Laguzzi, 1998). Euler integration is applied in time and upwind flux discretisation in space (Hirsch, 2007). The proposed staggered grid approach is shown in Figure 5.1. These numerical methods can capture shock waves, deal with discontinuities and ensure conditions for strict positive solutions.

[redacted]

Figure 5.1: Definition sketch of a staggered grid

The variables describing the internal and external flow area, concentration and bed level are calculated at the cell centres. The transport due to advection (flux) is calculated at the cell interfaces, see Figure 5.1. Water and sediment inflow as well as the sediment exchange fluxes are defined at the cell centres.

5.2 Boundary conditions and source/sink terms

The hopper is described by a closed domain (reflecting walls) and the resolution in the horizontal is defined by a series of layers of equal spatial distance (Δx). Water and bed level along the hopper is derived from continuity, therefore these boundaries are variable and explicitly calculated with time.

Source and sink terms

Water and sediment exchange within the external and internal current is modelled by defining source terms. The source terms describing the inflow and outflow discharge are only active at specific locations (cells). Depending on the spatial resolution these source terms are active at specific cells. Furthermore they can be activated at variable locations along the hopper length to consider different loading strategies. The effect of overflows is modelled as a sink term. These sinks can extract water and sediment from the schematization at their location (cells).

5.3 Initial conditions

The initial conditions and variables required to solve the hyperbolic set of equations are listed below:

- Bed level
- Water level
- External velocity
- External concentration
- Internal layer height
- Internal velocity
- Internal concentration

5.4 Numerical integration scheme

Here the numerical integration scheme to calculate the unknown variables for the internal and external water motion and suspended sediment transport as derived in section 3.1 & 3.2 is presented.

5.4.1 System of differential equations

The numerical scheme for the external and internal flow is presented by the one-dimensional equations for water-sediment mixture, sediment in the currents and the momentum equations. These one-dimensional equations are written in vector notation in conservative form as:

$$\frac{\partial \boldsymbol{V}}{\partial t}+\frac{\partial \boldsymbol{F}}{\partial x}=\boldsymbol{S} \tag{5.1}$$

Where **V** = vector of conserved variables, **F** = flux vector and **S** = source/sink vector. These vectors are presented below:

$$V=\begin{bmatrix} X \\ XX \\ XX \\ X \\ XX \\ XX \end{bmatrix}, \quad F=\begin{bmatrix} XX \\ XX \\ XX \\ XX \\ XX \\ XX+XX \end{bmatrix},$$

$$S=\begin{bmatrix} XX+XX+XX-XX-XX-XX \\ XX+XX+XX+XX-XX \\ XX-XXX \\ -XXX-XXX+XX+XXX \\ XXX+XXX+XXX-XXX-XXXX \\ XXXX+XXXXX-XXXX-XXX \end{bmatrix}$$

5.4.2 Discretization of the system of differential equations

The hyperbolic set of equations is discretised explicitly because of its simplicity, low internal memory usage and economical calculation time. Consequence of using an explicit scheme is a restriction to the time step to satisfy stability conditions (Hirsch, 2007). However, usually low Courant numbers are also required to achieve accurate results. The fully discretised external and internal mass- and momentum balance are presented below, note here the external momentum balance is discretised semi-implicit as will be elaborated in section 6.1. Note that the subscripts defining external or internal variables are neglected in the discretisation below.

Mass balance of the external water motion

$$XX = XX - XX[XX - XX] + XXX$$

$$V_i^n = A_i^n \qquad\qquad XX = XXX$$

$$F^n_{i+\frac{1}{2}} = \begin{cases} XXX & U^n_{i+1/2} > 0 \\ XXXX & U^n_{i+1/2} \leq 0 \end{cases} \tag{5.2}$$

$$F^n_{i-\frac{1}{2}} = \begin{cases} XXXX & U^n_{i-1/2} > 0 \\ XXXX & U^n_{i-1/2} \leq 0 \end{cases}$$

The discretised mass balance for positive flow is presented below:

$$\frac{A_i^{n+1} - A_i^n}{\Delta t} + \frac{(XX - XX)}{\Delta x} = S_i^n \tag{5.3}$$

Where the source/sink terms S_i^n are straightforward to discretise.

Momentum balance of the external water motion

$$XX = XX - XX[XX - XX] + XXX$$

$$V^n_{i-1/2} = U^n_{i-1/2} \qquad U_i^n = \frac{U^n_{i-1/2} + U^n_{i+1/2}}{2}$$

$$F_i^n = \begin{cases} XXXX & U_i^n > 0 \\ XXXX & U_i^n \leq 0 \end{cases} \tag{5.4}$$

$$F^n_{i-1} = \begin{cases} XXXX & U^n_{i-1} > 0 \\ XXXX & U^n_{i-1} \leq 0 \end{cases}$$

$$S^n_{i-1/2} = -cf\left|U^n_{i-1/2}\right|U^n_{i-1/2}P^n_{i-1/2}$$

The discretised explicit momentum balance for positive flow reads:

$$\frac{XX - XX}{\Delta t} + \frac{(XX - XX)}{\Delta x} + XX\frac{(XX - XX)}{\Delta x} + XXXXXX = 0 \tag{5.5}$$

XXXXXXXXXXXXXXXXXXXXXXXXXXXXXXXXXXXXXXXXXXXXXXXXXXXXXXXXXXXXXXXXXXXXXX XXXXXXXXXXXXXXXXXXXXXXXXXXXXXXXXXXXXXXXXXXXXXXXXXXXXXXXXXXXXXXXXX.

Suspended-sediment concentration balance of the external water motion

$$X = X - XX[XX - XX] + XX$$

$$V_i^n = XX$$

$$F^n_{i+\frac{1}{2}} = \begin{cases} XXXX & U^n_{i+1/2} > 0 \\ XXXXX & U^n_{i+1/2} \leq 0 \end{cases} \tag{5.6}$$

$$F^n_{i-\frac{1}{2}} = \begin{cases} XXXX & U^n_{i-1/2} > 0 \\ XXX & U^n_{i-1/2} \leq 0 \end{cases}$$

For positive flow the discretised concentration balance is written as:

$$XX = XX - XX[XX - XX] + XX$$

$$X = XX \cdot (XX - X[XXX - XXX] + XX) \tag{5.7}$$

Where the source/sink terms S_i^n are straightforward to discretise.

Mass balance of the internal water motion

$$XX = XX - XX[XX - XX] + XX$$

$$V_i^n = A_i^n \qquad A_{i+1/2}^n = \frac{A_i^n + A_{i+1}^n}{2}$$

$$F_{i+\frac{1}{2}}^n = \begin{cases} XX & U_{i+1/2}^n > 0 \\ XXX & U_{i+1/2}^n \leq 0 \end{cases} \tag{5.8}$$

$$F_{i-\frac{1}{2}}^n = \begin{cases} XX & U_{i-1/2}^n > 0 \\ XX & U_{i-1/2}^n \leq 0 \end{cases}$$

The discretised mass balance for positive flow is presented below:

$$\frac{A_i^{n+1} - A_i^n}{\Delta t} + \frac{(XXX - XXX)}{\Delta x} = S_i^n \tag{5.9}$$

Where the internal source/sink terms S_i^n are straightforward to discretise.

Momentum balance of the internal water motion

$$XX = XX - XX[X - X] + XX$$

$$V_{i-1/2}^n = U_{i-1/2}^n \qquad U_i^n = \frac{U_{i-1/2}^n + U_{i+1/2}^n}{2}$$

$$F_i^n = \begin{cases} XX & U_i^n > 0 \\ XX & U_i^n \leq 0 \end{cases} \tag{5.10}$$

$$F_{i-1}^n = \begin{cases} XX & U_{i-1}^n > 0 \\ XXX & U_{i-1}^n \leq 0 \end{cases}$$

The discretised explicit momentum balance for positive flow is presented below:

$$\frac{XX - XX}{\Delta t} + \frac{(XXX - XXX)}{\Delta x} + XXX\frac{(XXX - XXX)}{\Delta x} + XXXX\frac{(XX - XX)}{\Delta x} + XXXX\frac{(X - X)}{\partial x} = S_{i-1/2}^n \tag{5.11}$$

Suspended-sediment concentration balance of the internal water motion

$$XX = XX - XX[XX - XX] + XXX$$

$$V_i^n = (\phi_i A_i)_i^n$$

$$F^n_{i+\frac{1}{2}} = \begin{cases} XXX & U^n_{i+1/2} > 0 \\ XXXX & U^n_{i+1/2} \le 0 \end{cases} \qquad (5.12)$$

$$F^n_{i-\frac{1}{2}} = \begin{cases} XXX & U^n_{i-1/2} > 0 \\ XXX & U^n_{i-1/2} \le 0 \end{cases}$$

For positive flow the discretised concentration balance is written as:

$$XX = XX - XX[XXX - XXX] + XXX$$

$$XX = XX \cdot (XX - XX[XXX - XXX] + XX) \qquad (5.13)$$

Where the source/sink terms S_i^n are straightforward to discretise.

5.3.1 Stability Criteria

The discretised explicit upwind scheme is first order accurate. Therefore, to ensure stable calculations, the Courant (Hirsch, 2007) stability criterion should be satisfied:

$$C_r = \left(\frac{(U + c) \cdot \Delta t}{\Delta x}\right)_{max} \tag{5.14}$$

$$with\ c = c_e = \sqrt{gH}\ or\ c_i = \alpha\sqrt{\varepsilon g h} \quad where\ 0 < C_r < 1$$

Where H is the total flow depth, h is the internal layer depth, U is either the external or internal flow velocity and c the external or internal wave propagation speed. It is clear that the external water motion determines what time step to apply, given the model schematization ($H \gg h$), to satisfy the Courant condition.

First order upwind discretisation of the continuity equation causes numerical diffusion depending on the mesh and time step. Magnitude of the numerical diffusion can be determined by introducing Taylor expansion to the linear advection equation (Hirsch, 2007):

$$\frac{\partial A_e}{\partial t} + U_e \frac{\partial A_e}{\partial x} = \frac{U_e \Delta x}{2}\left(1 - \frac{U_e \Delta t}{\Delta x}\right)\frac{\partial^2 A_e}{\partial x^2} \equiv D_{num}\frac{\partial^2 A_e}{\partial x^2} \tag{5.15}$$

Where D_{num} is the numerical diffusion coefficient. Due to the first order upwind discretisation the magnitude of numerical diffusion has to be limited by choosing a favourable spatial resolution.

6 Model verification to analytical solutions

The discretization of the individual terms in the conservation balances are tested for conservation, monotonicity at steep gradients and stability against analytical results of several idealized case studies. Because the proposed model is divided in a two-layer framework (barotropic and baroclinic flow) firstly case studies describing the external (barotropic) flow are performed and verified followed by test cases for the internal (baroclinic) current.

6.1 XXXXXXXXXXXXXXXXX

XXXXXXXXXXXXXXXXXXXXXXXXXXXXXXXXXXXXXXXXXXXXXXXXXXXXXXXXXXXXXXXXXXXXXX XXXXXXXXXXXXXXXXXXXXXXXXXXXXXXXXXXXXXXXXXXXXXXXXXXXXXXXXXXXXXXXXXXXXXX XXXXXXXXXXXXXXXXXXXXXX.

6.1.1 Description of the case

XXXXXXXXXXXXXXXXXXXXXXXXXXXXXXXXXXXXXXXXXXXXXXXXXXXXXXXXXXXXXXXXXXXXXX XXXXXXXXXXXXXXXXXXXXXXXXXXXXXXXXXXXXXXXXXXXXXXXXXXXXXXXXXXXXXXXXXXXXXX XXXXXXXXXXXXXXXXXXXXXXXXXXXXXXXXXXXXXXXXXXXXXXXXXXXXXXXXXXXXXXXXXXXXXX XXXXXXXXXXXXXXXXXXXXXXXXXXXXXXXXXXXXXXXXXXXXXXXXXXXXXXXXXXXX.

(a)

[redacted]

(b)

[redacted]

Figure 6.1: Sketch of dam break simulation (a) initial situation, (b) front propagation

XXXXXXXXXXXXXXXXXXXXXXXXXXXXXXXXXXXXXXXXXXXXXXXXXXXXXXXXXXXXXXXXXXXXXX XXXXXXXXXXXXXXXXXXXXXXXXXXXXXXXXXXXXXXXXXXXXXXXXXXXXXXXXXXXXXXXXXXXXXX XXXXXXXXXXXXXXXXXXXXXXXXXXXXXXXXXXXXXXXXXXXXXXXXXXXXXXXXXXXXXXXXXXXXXX XXXXXXXXXXXXXXXXXXXXXXXXXXXXXXXXXXXXXXXXXXXXXXXXXXXXXXXXXXXXXXXXXXXXXX XXXXXXXXXXXXXXXXXXXXXXXXXXXXXXXXXXXXXXXXXXXXXXXXXXXXX.

6.1.2 XXXXXXXXXXXXXXXXXXXXXXXXXXX

XXXXXXXXXXXXXXXXXXXXXXXXXXXXXXXXXXXXXXXXXXXXXXXXXXXXXXXXXXXXXXXXXXXXXXXXX XXXXXXXXXXXXXXXXXXXXXXXXXXXXXXXXXXXXXXXXXXXXXXXXXXXXXXXXXXXXXXXXXXXXXXXXX XXXXXXXXXXXXXXXXXXXXXXXXXXXXXXXXXXXXXXXXXXXXXXXXXXXXXXXXXXXXXXXXXXXXXXXXX XXXXXXXXXXXXXXXXXXXXXXXXXXXXXXXXXXXXXXXXXXXXXXXXXXXXXXXXXXXXXXXX:

$$\frac{\partial \boldsymbol{V}}{\partial t} + \frac{\partial \boldsymbol{F}}{\partial x} = \boldsymbol{S} \tag{6.1}$$

$$V = \begin{bmatrix} XX \\ XX \end{bmatrix}, \qquad F = \begin{bmatrix} XX \\ XXX \end{bmatrix}, \qquad S = \begin{bmatrix} X \\ XXXX \end{bmatrix} \tag{6.2}$$

XXXXXXXXXXXXXXXXXXXXXXXXXXXXXXXXXXXXXXXXXXXXXXXXXXXXXXXXXXXXXXXXXXXXXXXXX XXXXXXXXXXXXXXXXXXXXXXXXXXXXXXXXXXXXXXXXXXXXXXXXXXXXXXXXXXXXXXXXXXXXXXXXX XXXXXXXXXXXXXXXXXXXXXXXXXXXXXXXXXXXXXXXXXXXXXXXXXXXXXXXXXXXXXXXXXXXXXXXXX XXXXXXXXXXXXXXXXXXXXXXXXXXXXXXXXXXXXXXXXXXXXXXXXXXXXXXXXXXXXXXXXXXXXXXXXX XXXXXXXXXXXXXXXXXXXXXXXXXXXXXXXXXXXXXXXXXXXXXXXXXXXXX

XXXXXXXXXXXXXXXXXXXXXXXXXXXXXXXXXXXXXXXXXXXXXXXXXXXXXXXXXXXXXXXXXXXXXXXXX XXXXXXXXXXXXXXXXXXXXXXXXXXXXXXXXXXXXXXXXXXXXXXXXXXXXXXXXXXXXXXXXXXXXXXXX XXXXXXXXXXXXXXXXXXXXXXXXXXXXXXXXXXXXXXXXXXXXXXXXXXXXXXXXXXXXXXXXXXXXXXXXX XXXXXXXXXXXXXXXXXXXXXXXXXXXXXXXXXXXXXXXXXXXXXXXXXXXXXXXXXXXXXXXXXXXXXXXXX XXXXXXXXXXXXXXXXXXXXXXXXXXXXXXXXXXXXXXXXXXXXXXXXXXXXXXXXXXXXXXXXXXXXXXXXX XXXXXXXXXXXXXXXXXXXXXXXXXXXXXX:

$$XXXXXXXXXXXXXXXXXXXXXXX \tag{6.3}$$

$$XXXXXXXXXXXXXXXXX \tag{6.4}$$

$$XXXXXXXXXXX \tag{6.5}$$

XXXXXXXXXXXXXXXXXXXXXXXXXXXXXXXXXXXXXXXXXXXXXXXXXXXXXXXXXXXXXXXXXXXXXXXXX

XXXXXXXXXXXXXXXXXXXXXXXXXXXXXXXXXXXXXXXXXXXXXXXXXXXXXXXXXXXXXXXXXXXXXXXXX XXXXXXXXXXXXXXXXXXXXXXXXXXXXXXXXXXXXXXXXXXXXXXXXXXXXXXXXXXXXXXXXXXXXXXXXX XXXXXXXXXXXXXXXXXXXXXXXXXXXXXXXXXXXXXXXXXXXXXXXXXXXXXXXXXXXXXXXXXXXXXXXXX

XXXXXXXXXXXXXXXXXXXXXXXXXXXXXXXXXXXXXXXXXXXXXXXXXXXXXXXXXXXXXXXXXXXXXXXXX XXXXXXXXXXXXXXXXXXXXXXXXXXXXXXXXXXXXXXXXXXXXXXXXXXXXXXX:

$$X = XXXXXXXXX \tag{6.6}$$

$$X = XXXXXX \tag{6.7}$$

6.1.3 XXXXXXXXXXXXXXXXXXXXXXXXXXXXXXXXXXXX

XXXXXXXXXXXXXXXXXXXXXXXXXXXXXXXXXXXXXXXXXXXXXXXXXXXXXXXXXXXXXXXXXXXXXXXX XXXXXXXXXXXXXXXXXXXXXXXXXXXXXX:

$$\frac{XXX - XXXX}{\Delta t} + \left[\frac{XXX}{\Delta x} - \frac{XXX}{\Delta x}\right] + XX\frac{(X - X)}{\Delta x} = 0 \tag{6.8}$$

XXXXXXXXXX:

$$X = XX + XXX, \qquad XX = \frac{X + X}{2}, \qquad X = \frac{XX + XX}{2}$$

XXXXXXXXXXXXXXXXXXXXXXXXXXXXXXXXXXXXXXXXXXXXXXXXXXXXXXXXXXXXXXXXXXXXXXXX XXXXXXXXXXXXXXXXXXXXXXXXXXXXXXXXXXXXXXXXXXXXXXXXXXXXXXXXXXXXXXXXXXXXXXX.

XXXXXXXXXXXXXXXXXXXXXXXXXXXXXXXXXXXXXXXXXXXXXXXXXXXXXXXXXXXXXXXXXXXXXXXX XXXXXXXXXXXXXXXXXXXXXXXXXXXXXXXXXXXXXXXXXXXXXXXXXXXXXXXXXXXXXXXXXXXXXXXX XXXXXXXXXXXXXXXXXXXXXXXXXXXXXXXXXXXXXXXXXXXXXXXXXXXXXXXXXXXXXXXXXXXXXXXX XXXXXXXXXXXXXXXXXXXXXXXXXXXXXXXXXXXXXXXXXXXXXXXXXXXXXXXXXXXXXXXXXXXXXXXX XXXXXXXXXXXXXXXXXXXXXXXXXXXXXXXXXXXXXXXXXXXXXXXXXXXXXX.

XXXXXXXXXXXXXXXXXXXXXXXXXXXXXXXXXXXXXXXXXXXXXXXXXXXXXXXXXXXXXXXXXXXXXXXX XXXXXXXXXXXXXXXXXXXXXXXXXXXXXXXXXXXXXXXXXXXXXXXXXXXXXXXXXXXXXXXXXXXXXXXX XXXXXXXXXXXXXXXXXXXXXXXXXXXXXXXXXXXXXXXXXXXXXXXXXXXXXXXXXXXXXXXXXXXXXXXX XXXXXXXXXXXXXXXXXXXXXXXXXXXXXXXXXXXXXXXXXXXXXXXXXXXXX.

(a) (b)

[redacted]

Figure 6.2: XXXXXXXXXXXXXXXXXXXXXXXXXXXXXXXXXXXXXXXXXXXXXXXXXXXXXXXXXXXXXXXXXXXXXX.

XXXXXXXXXXXXXXXXXXXXXXXXXXXXXXXXXXXXXXXXXXXXXXXXXXXXXXXXXXXXXXXXXXXXXXXX XXXXXXXXXXXXXXXXXXXXXXXXXXXXXXXXXXXXXXXXXXXXXXXXXXXXXXXXXXXXXXXXXXXXXXXX XXXXXXXXXXXXXXXXXXXXXXXXXXXXXXXXXXXXXXXXXXXXXXXXXXXXXXXXXXXXXXXXXXXXXXXX XXXXXXXXXXXXXXXXXXXXXXXXXXXXXXXXXXXXXXXXXXXXXXXXXXXXXXXXXXXXXXXXXXXXXXXX XXXXXXXXXXXXXXXXXXXXXXXXXXXXXXXXXXXXXXXXXXXXXXXXXXXXXXXXXXXXXXXXXXXXXXXX XXXXXXXXXXXXXXXXXXXXXXXXXXXXXXXXXXXXXXXXXXXXXXXXXXXXXXXXXXXXXXXXXXXXXXXX XXXXXXXXXXXXXXXXXXXXXXXXXXXXXXXXXXXXXXXXXXXXXXXXXXXXXXXXXXXXXXXXXXXXXXXX XX.

XXXXXXXXXXXXXXXXXXXXXXXXXXXXXXXXXXXXXXXXXXXXXXXXXXXXXXXXXXXXXXXXXXXXXXX XXXXXXXXXXXXXXXXXXXXXXXXXXXXXXXXXXXXXXXXXXXXXXXXXXXXXXXXXXXXXXXXXXXXXXX XXXXXXXXXXXXXXXXXXXXXXXXXXXXXXXXXXXXXXXXXXXXXXXXXXXXXXXXXXXXXXXXXXXXXXX XXXXXXXXXXXXXXXXXXXXXXXXXXXXXXXXXXXXXXXXXXXXXXXXXXXXXXXXXXXXXXXXXXXXXXX XXXXXXXXXXXXXXXXXXXXXXXXXXXXXXXXXXXXXXXXXXXXXXXXXXXXXX.

(a) (b)

[redacted] [redacted]

Figure 6.3: XXXXXXXXXXXXXXXXXXXXXXXXXXXXXXXXXXXXXXXXXXXXXXXXXXXXXXXXXXXXXXXXX.

XXXXXXXXXXXXXXXXXXXXXXXXXXXXXXXXXXXXXXXXXXXXXXXXXXXXXXXXXXXXXXXXXXXXXXX XXXXXXXXXXXXXXXXXXXXXXXXXXXXXXXXXXXXXXXXXXXXXXXXXXXXXXXXXXXXXXXXXXXXXXX XXXXXXXXX.

XXXXXXXXXXXXXXXXXXXXXXXXXXXXXXXXXXXXXXXXXXXXXXXXXXXXXXXXXXXXXXXXXXXXXXX XXXXXXXXXXXXXXXXXXXXXXXXXXXXXXXXXXXXXXXXXXXXXXXXXXXXXXXXXXXXXXXXXXXXXXX XXXXXXXXXXXXXXXXXXXXXXXXXXXXXXXXXXXXXXXXXXXXXXXXXXXXXX.

(a) (b)

[redacted] [redacted]

Figure 6.4: XXXXXXXXXXXXXXXXXXXXXXXXXXXXXXXXXXXXXXXXXXXXXXXXXXXXXXXXXXXXXXXXXXXXX.

XXXXXXXXXXXXXXXXXXXXXXXXXXXXXXXXXXXXXXXXXXXXXXXXXXXXXXXXXXXXXXXXXXXXXXX XXXXXXXXXXXXXXXXXXXXXXXXXXXXXXXXXXXXXXXXXXXXXXXXXXXXXXXXXXXXXXXXXXXXXXX XXXXXXXXXXXXXXXXXXXXXXXXXXXXXXXXXXXXXXXXXXXXXXXXXXXXXXXXXXXXXXXXXXXXXXX XXXXXXXXXXXXXXXXXXXXXXXXXXXXXXXXXXXXXXXXXXXXXXXXXXXXXXXXXXXXXXXXXXXXXXX

XXXXXXXXXXXXXXXXXXXXXXXXXXXXXXXXXXXXXXXXXXXXXXXXXXXXXXXXXXXXXXXXXXXXX
XXXXXXXXXXXXXXXXXXXXXXXXXXXX.

XXXXXXXXXXXXXXXXXXXXXXXXXXXXXXXXXXXXXXXXXXXXXXXXXXXXXXXXXXXXXXXXXXXXX
XXXXXXXXXXXXXXXXXXXXXXXXXXXXXXXXXXXXXXXXXXXXXXXXXXXXXXXXXXXXXXXXXXXXX
XXXXXXXXXXXXXXXXXXXXXXXXXXXXXXXXXXXXXXXXXXXXXXXXXXXXXXXXXXXXXXXXXXXXX
XXXXXXXXXXXXXXXXXXXXXXXXXXXXXXXXXXXXXXXXXXXXXXXXXXXXXXXXXXXXXXXXXXXXX
XXXXXXX:

$$\Rightarrow XXX \qquad ,XXXX \tag{6.9}$$

XXXXXXXXXXXXX

XXXXXXXXXXXXXXXXXXXXXXXXXXXXXXXXXXXXXXXXXXXXXXXXXXXXXXXXXXXXXXXXXXXXX
XXXXXXXXXXXXXXXXXXXXXXXXXXXXXXXXXXXXXXXXXXXXXXXXXXXXXXXX.

(a) [redacted]

(b) [redacted]

Figure 6.5XXXXXXXXXXXXXXXXXXXXXXXXX.

XXXXXXXXXXXXXXXXXXXXXXXXXXXXXXXXXXXXXXXXXXXXXXXXXXXXXXXXXXXXXXXXXXXXX
XXXXXXXXXXXXXXXXXXXXXXXXXXXXXXXX:

$$\Rightarrow XXXXX \qquad if\ XXXX \tag{6.10}$$

XXXXXXXXXXXXXXXXXXXXXXXXXXXXXX

XXXXXXXXXXXXXXXXXXXXXXXXXXXXXXXXXXXXXXXXXXXXXXXXXXXXXXXXXXXXXXXXXXXXX
XXXXXXXXXXXXXXXXXXXXXXXXXXXXXXXXXXXXXXXXXXXXXXXXXXXXXXXXXXXXXXXXXXXXX
XXXXXXXXXXXXXXXXXXXXXXXXXXXXXXXXXXXXXXXXXXXXXXXXXXXXXXXXXXXXXXXXXXXXX
XXXXXXXXXXXXXXXXXXXXXXXXXXXXXXXXXXXXXXXXXXXXXXXXXXXXXXXXXXXXXXXXXXXXX
XXXXXXXXXXXXXXXXXXXXXXXXXXXXXXXXXXXXXXXXXXXXXXXXXXXXXXXXXXXXXXXXXXXXX
XXXXXXXXXXXXXXXXXXXXXXXXXXXXXXXXXXXXX:

(a) (b)

[redacted]

Figure 6.6: XXXXXXXXXXXXXXXXXXXXXXXXXXXXXXXXXXXXXXXXXXXXXXXXXXXXXXXXXXXXXXXXXXXX.

6.2 Subcritical flow over bed profile, mass and energy conservation

Here, the discretised external model is tested for an incompressible frictionless steady state flow over a continuous- and discontinuous bed profile to examine whether conservation of mass and mechanical energy is satisfied or not. This type of a problem can be analytically solved with Bernoulli's equation. This equation can be derived from Euler's one-dimensional non-viscous equation of motion with assumption of steady state incompressible flow. Bernoulli's equation can be viewed as the conservation of mechanical energy: the sum of the kinetic (velocity head), potential (elevation head), and flow energies (pressure head) of a fluid particle is constant along a streamline during steady state flow without the effects of compressibility and friction.

Note that a deformation in the bed profile can cause the development of a transition from sub critical into supercritical flow or vice versa.

The continuous bed profile is defined as follows:

$$d(x) = \begin{cases} 0.2m - 0.05m(x-10m)^2, & if\ 8m < x < 12m \\ 0m, & otherwise \end{cases} \tag{6.11}$$

Discontinuous bed profile is defined as:

$$d(x) = \begin{cases} 0.2m, & if\ 8m < x < 12m \\ 0m, & otherwise \end{cases} \tag{6.12}$$

Conservation of mechanical energy is satisfied along a streamline if the following equation is satisfied (Bernoulli):

$$\frac{\partial}{\partial x}\left(\frac{1}{2}u^2 + \frac{p}{\rho} + gz\right) = 0 \tag{6.13}$$

Subcritical flow over continuous bed profile

For this test problem a constant discharge is specified at the upstream side of the domain and a fixed water level at the downstream side equal to $4.42\ m^3/s$ and 2.0 m., respectively. The width 1.0 m. and constant over the entire length of the domain of 25 m.

Figure 6.7 shows the water level and discharge profile of a subcritical steady state flow over a continuous (bump) bed profile. As the results represent the numerical solution shows accurate agreement with the analytical solution. Water level profile shows locally a contraction in height at the location of the bed profile.

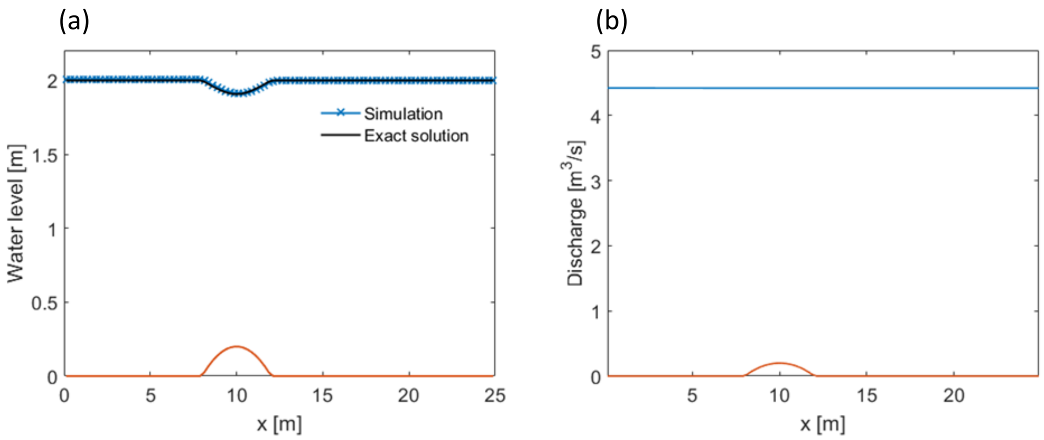

Figure 6.7: Numerical simulation steady state subcritical flow over a bump after 100 s. Graph (a) shows water level profile, graph (b) shows the discharge along the length.

Due to the bump in the bed profile the flow over the bump accelerates and decelerates. This causes a water level depression over the length of the bump with a minimum at the centre of the bump. The explanation for this is, based on Bernoulli's theorem, that the kinetic energy (velocity head) increases at the bump at the expense of flow energy (pressure head). Thus, the pressure head at the bumps drops and hence the water level.

Supercritical flow over continuous smooth bed topography

Figure 6.8 shows a simulation of a steady state transition from a subcritical flow to a supercritical flow over a continuous smooth bed profile. A discharge of 1,53 m^3/s at the upstream boundary is imposed and the initial water level is equal to 0.40m. and zero flow (velocity).

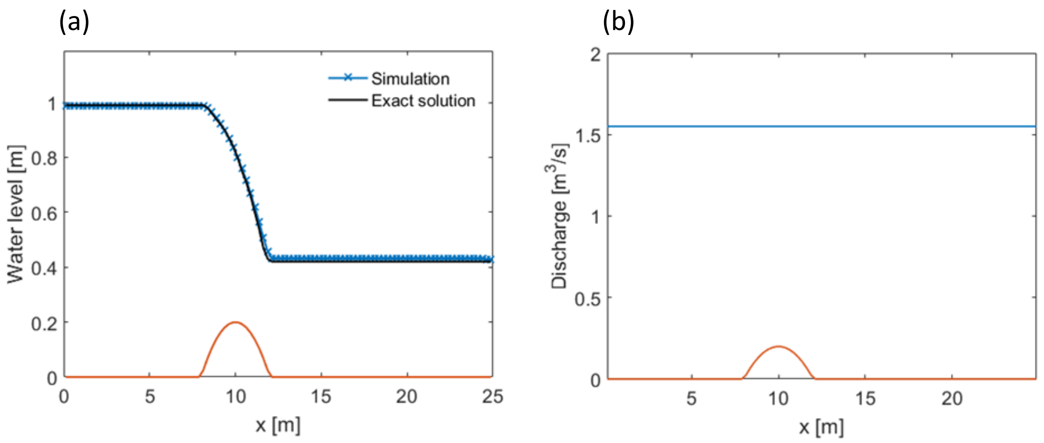

Figure 6.8: Numerical simulation of steady state subcritical flow over a bump after 100 s. Graph (a) shows the water level profile, graph (b) shows the water discharge along the domain.

Figure 6.8 shows accurate agreement with the analytical solution. This means that energy is accurately conserved and that the model can deal with the transition sub- to supercritical flow. The horizontal discharge is constant along the entire length of the domain (Figure 6.8 (b)) which means that mass is appropriately conserved.

Supercritical flow with discontinuous "sharp" bed profile

A supercritical flow over a discontinues sharp bed profile is performed to examine the discretised scheme can deal with sharp bed slope gradients. A discharge of $0.18\ m^3/s$ at the upstream side is imposed and at the downstream side the water level is fixed at 0.275m. The length of the domain is 25 m and the spatial- and time step are dx = 0.25m and dt = 0.01.

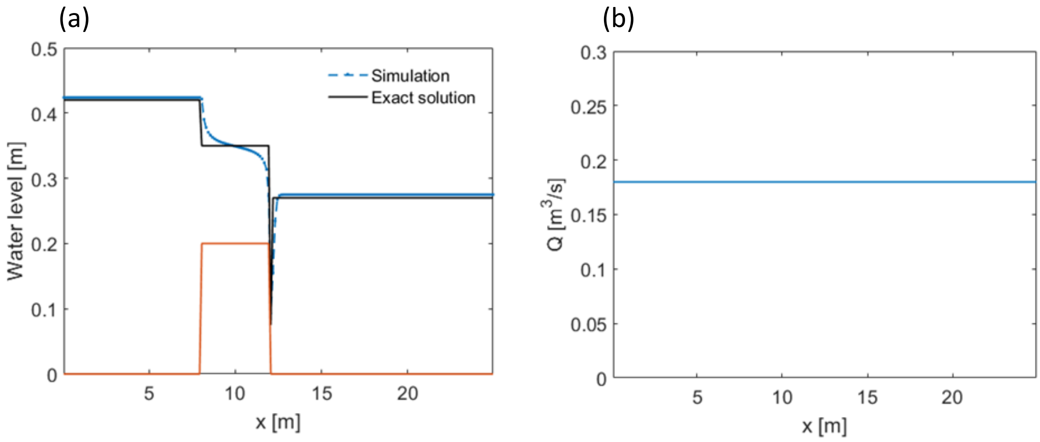

Figure 6.9: Numerical simulation steady state solution of a supercritical flow over a discontinuous bed profile. Graph (a) shows the water level profile, graph (b) shows the discharge through the domain.

Figure 6.9 shows the results of the steady state solution of the supercritical flow over a discontinues bed profile. The simulation fulfils conservation of mass concluded from the constant discharge profile shown by Figure 6.9 (b). The numerical solution reproduce accurate agreement with the analytical solution, only near steep gradients the solution shows smooth transitions. This is a cause of numerical (artificial) diffusion due to the first order scheme (Hirsch, 2007).

XXXXXXXXXXXXXXXXXXXXXXX

XXXXXXXXXXXXXXXXXXXXXXXXXXXXXXXXXXXXXXXXXXXXXXXXXXXXXXXXXXXXXXXXXXXXXXX XXXXXXXXXXXXXXXXXXXXXXXXXXXXXXXXXXXXXXXXXXXXXXXXXXXXXXXXXXXXXXXXXXXXXXX XXXXXXXXXXXXXXXXXXXXXXXXXXXXXXXXXXXXXXXXXXXXXXXXXXXXXXXXXXXXXXXXXXXXXXX XXXXXXXXXXXXXXXXXXXXXXXXXXXXXXXXXXXXXXXXXXXXXXXXXXXXXXXXXXXXXXXXXXXXXXX XXXXXXXXXXXXXXXXXXXXXXXXXXXXXXXXXXXXXXXXXXXXXXXXXXXXXX:

$$XX = XXXXXXXXXXXXXX \tag{6.14}$$

XXXXXXXXXXXXXXXXXXXXXXXXXXXXXXXXXXXXXXXXXXXXXXXXXXXXXXXXXXXXXXXXXXXXXXX XXXXXXXXXXXXXXXXXXXXXXXXXXXXXXXXXXXXXXXXXXXXXXXXXXXXXXXXXXXXXXXXXXXXXXX XXXXXXXXXXXXXXXXXXXXXXXXXXXXXX:

$$X = XX \tag{6.15}$$

XXXXXXXXXXXXXXXXXXXXXXXXXXXXXXXXXXXXXXXXXXXXXXXXXXXXXXXXXXXXXXXXXXXXXXX XXXXXXXXXXXXXXXXXXXXXXXXXXXXXXXXXXXXXXXXXXXXXXXXXXXXXXXXXXXXXXXXXXXXXXX XXXXXXXXXXXXXXXXXXXXXXXXXXXXXXXXXXXXXXXXXXXXXXXXXXXXXXXXXXXXXXXXXXXXXXX XXXXXXXXXXXXXXXXXXXXXXXXXXXXXXXXXXXXXXXX.

XXXXXXXXXXXXXXXXXXXXXXXXXXXXXXXXXXXXXXXXXXXXXXXXXXXXXXXXXXXXXXXXXXXXXXX XXXXXXXXXXXXXXXXXXXXXXXXXXXXXXXXXXXXXXXXXXXXXXXXXXXXXXXXXXXXXXXXXXXXXXX XXXXXXXXXXXXXXXXXXXXXXXXXXXXXXXXXXXXXXXXXXXXXXXXXXXXXXXXXXXXXXXXXXXXXXX XXXXXXXXXXXXXXXXXXXXXXXXXXXXXXXXXXXXXXXXXXXXXXXXXX.

$$XXXXXXXXXXXXXXXXXXXXXXXXXXXXXXXXXXXXX.$$

(a) [redacted]

(b) [redacted]

Figure 6.10: XXXXXXXXXXXXXXXXXXX

XXXXXXXXXXXXXXXXXXXXXXXXXXXXXXXXXXXXXXXXXXXXXXXXXXXXXXXXXXXXXXXXXXXXXXX XXXXXXXXXXXXXXXXXXXXXXXXXXXXXXXXXXXXXXXXXXXXXXXXXXXXXXXXXXXXXXXXXXXXXX XXXXXXXXXXXXXXXXXXXXXXXXXXXXXXXXXXXXXXXXXXXXXXXXXXXXXXXXXXXXXXXXXXXXXX XXXXXXXXXXXXXXXXXXXXXXXXXXXXXXXXXXXXXXXXXXXXXXXXXXXXXXXXXXXXXXXXXXXXXXX.

XXXXXXXXXXXXXXXXXXXXXXXXXXXXXXXXXXXXXXXXXXXXXXXXXXXXX.

[redacted]

Figure 6.11: XXXXXXXXXXXXXXXXXXXXXXXXXXXXXXXXXXXXXXXXXXXXXXXXXXXXXXXXXXXXXXXXXX.

XXXXXXXXXXXXXXXXXXXXXXXXXXXXXXXXXXXXXXXXXXXXXXXXXXXXXXXXXXXXXXXXXXXXXXX XXXXXXXXXXXXXXXXXXXXXXXXXXXXXXXXXXXXXXXXXXXXXXXXXXXXXXXXXXXXXXXXXXXXXXX XXXXXXXXXXXXXXXXXXXXXXXXXXXXXXXXXXXXXXXXXXXXXXXXXXXXXXXXXXXXXXXXXXXXXXX XXXXXXXXXXXXXXXXXXXXXXXXXXXXXXXXXXXXXXXXXXXXXXXXXXXXXXXXXXXXXXXXXXXXXXX XXXXXXXXXXXXXXXXXXXXXXXXXXXXXXXXXXXXXXXXXXXXXXXXXXXXX.

6.3 Water inflow (external layer)

Here water discharge into a closed domain (rectangular domain) is examined to verify proper implementation of the inflowing source terms and reflecting boundary walls. Furthermore this test verifies proper propagation/filling of the water motion for different (left, right, middle) discharge location(s). Filling of the domain is modelled by adding a source term in the continuity equation.

A water discharge equal to $8\ m^3/s$ is imposed at pre-defined locations along the domain. A square box with length L=100m., a constant width B=5m and an initial water level inside the box of 3.0m is defined. The discharge source term is included to the continuity equation as defined in section 3.1.1:

$$\frac{\partial A_e}{\partial t} + \frac{\partial A_e U_e}{\partial x} = P_{lp;w,e} B \tag{6.16}$$

Where $P_{lp;w,e}$ is the water discharge source term and B is the width of the free surface at the loading location.

Figure 6.12 shows the results of water discharge into the domain at four different locations; left, right, middle and both left and right.

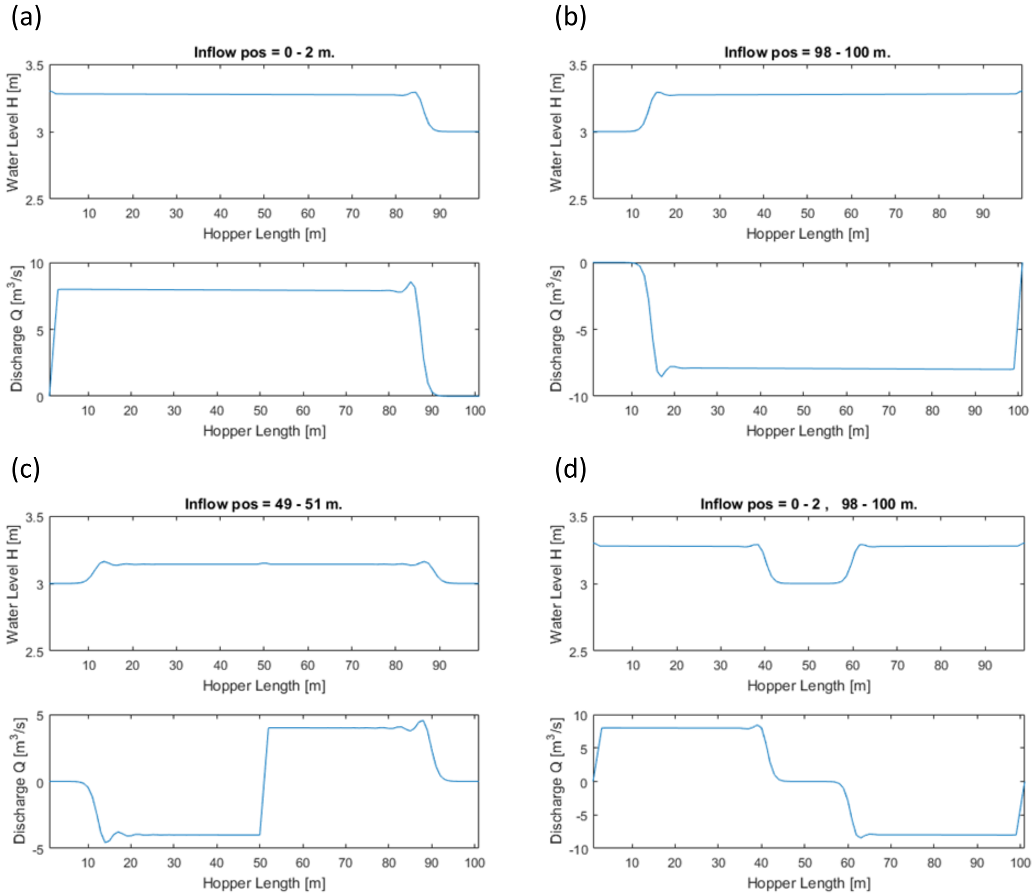

Figure 6.12: Four test cases each showing water level and discharge along the hopper length where the discharge location is varied. Graph (a) represents discharge position x =0 and t =15 s, graph (b) represents discharge position x =100 and t = 15 s, graph (c) represents discharge position x =50 m and t = 7 s. and graph (d) represents discharge location at x = 0 and x = 100 m. Δx = 1.0 m, Δt = 0.05 s and chezy roughness coefficient C = 40.

The model runs stable for discharge positions located at different location along the hopper length or with multiple discharge positions. Mass is conserved within this framework calculated with the mass balance as presented below:

$$M_{final} = M_{begin} + \rho_w \int_{t_0}^{t_1} Q_{in} dt \tag{6.17}$$

Where M_{begin} is the mass inside the domain before filling and Q_{in} is the water discharge into the domain.

6.4 Sedimentation Length

Previous test cases verified proper propagation of the external water motion defined by conservation of mass, momentum and energy.

An analytical solution for the sedimentation length of suspended sand is derived based on concentration transport by horizontal (1D) advection. Assume steady state conditions, this means constant discharge $q[m^2/s]$ throughout the domain. Impose a constant concentration discharge ϕ_0 at the upstream boundary, constant settling velocity w_s throughout the domain and constant width B. The (1D) horizontal concentration advection equation reads:

$$\frac{\partial \phi h}{\partial t} + \frac{\partial \phi q}{\partial x} = -w_s \phi \tag{6.18}$$

$$q \frac{d\phi}{dx} + w_s \phi = 0 \tag{6.19}$$

$$\frac{\phi}{\phi_0} = \exp\left(-\frac{x}{L_{sed}}\right) \tag{6.20}$$

Where L_{sed} is defined as the sedimentation length:

$$L_{sed} = \frac{q}{w_s} \tag{6.21}$$

$$at\ x = L_{sed}\ \Rightarrow 1 - e^{-1} = 63.2\%\ of\ the\ suspended\ sediment\ is\ settled$$

Impose a constant discharge per unit width of $q = 10\, m^2/s$ with a constant concentration of $\phi = 0.2$ and a settling velocity $w_s = 1.0\, m/s$. The length of the domain is 100 m. and the simulation time is 50 s.

Figure 6.13 shows the results of the normalised concentration profile compared with the analytical solution (Eq. 6.20) of four test cases with variation in number of grid cells (25, 50, 100 and 200).

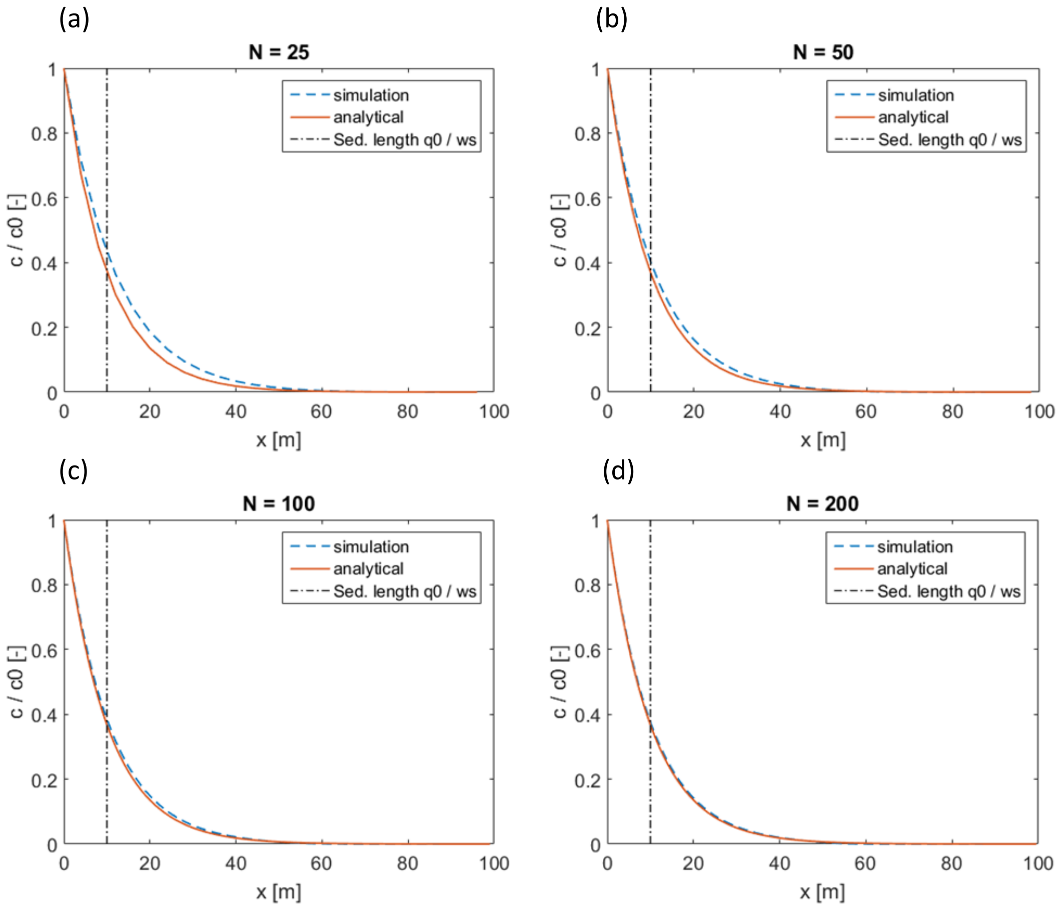

Figure 6.13: Simulations of concentration profile against analytical solution for respectively the number of grid cells equal to N=25, N=50, N=100 and N=200.

The result shows that with increasing number of grids cells the numerical solution converges towards the analytical solution. At low spatial resolution less sediment settles which is caused by numerical diffusion (first order upwind discretisation). With increasing spatial resolution the numerical simulation shows accurate agreement with the analytical solution. Hence suspended sediment is correctly transported through the domain.

6.5 Density driven exchange current, momentum conservation

Previous test cases were performed to verify proper conservation of the external (barotropic) water motion. It is verified that the developed model satisfies these laws. This means the external layer is now fully verified. Now the internal (barotropic) water motion has to be verified against idealised analytical solutions.

In this section the dynamical behaviour of an axis-symmetric density (internal) driven exchange current is examined over a horizontal bed. Furthermore the propagation of a density current over a sloping bed is simulated to verify the discretised scheme can deal with bed gradients. Both these cases are performed with a lock gate simulation separating a denser fluid from a less dense overlaying fluid, after releasing the lock gate a density currents starts to propagate horizontally along the bed.

6.5.1 Density driven exchange current over a horizontal bed

The fully set of conservation equations to describe the internal water motion are derived in Chapter 0. The governing conservation equations terms to describe the frictionless density current over a horizontal bed are presented below in vector notation:

$$V = \begin{bmatrix} A_i \\ U_i A_i \end{bmatrix}, \qquad F = \begin{bmatrix} A_i U_i \\ U_i A_i U_i + \frac{1}{2}\varepsilon g h A_i \end{bmatrix}, \qquad S = \begin{bmatrix} 0 \\ \frac{1}{2}\frac{\rho_e}{\rho_i} g \frac{\partial H A_i}{\partial x} \end{bmatrix} \tag{6.22}$$

XXXXXXXXXXXXXXXXXXXXXXXXXXXXXXXXXXXXXXXXXXXXXXXXXXXXXXXXXXXXXXXXXXXX XXXXXXXXXXXXXXXXXXXXXXXXXXXXXXXXXXXXX:

$$XX = XXXXXXXXXXXX \tag{6.23}$$

XXXXXXXXXXXXXXXXXXXXXXXXXXXXXXXXXXXXXXXXXXXXXXXXXXXXXXXXXXXXXXXXXXXX XXXXXXXXXXXXXXXXXXXXXXXXXXXXXXXXXXXXXXXXXXXXXXXXXXXXXXXXXXXXXXXXXXXX XXXXXXXXXXXXXXXXXXXXXXXXXXXXXXXXXXXXXXXXXXXXXXXXXXXXXXXXXXXXXXXXXXXX XXXXXXXXXXXXXXXXXXXXXXXXXXXXXXXXXXXXXXXXXXXX.

To simulate a density driven exchange flow the following problem is examined. The initial density of the block of dense fluid behind the lock is 1187.5 kg/m^3 based on a solids concentration of 0.1 [-]. The lock length and height are 25m. and 3.0m., respectively. Length of the domain is 2000m where the grid size is equal to N = 2*83 and the time step equals dt = 2 s. The height of the ambient water column is considered large to neglect the influence of the ambient water layer.

Figure 6.14 shows the dynamical development of the propagating density front position in time. Graphs (a) and (b) show respectively the height and velocity profile of the propagating front after simulation of 200s. Graph (c) shows the total front distance travelled compared with the analytical expression as presented in Eq. 6.24 on log-log scale.

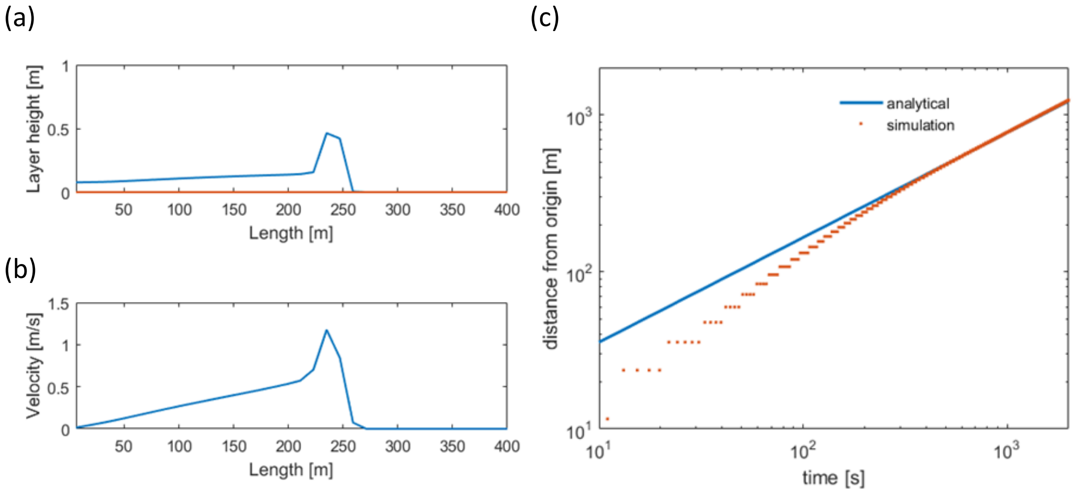

Figure 6.14: Graph a shows the layer height profile of the lock exchange current after simulation of 200s. Graph b shows the velocity profile of the lock exchange current. Graph c shows the front propagation of the internal current in time in log-log scale compared with the analytical solution.

By releasing the lock gate a slumping phase can be perceived where the block of denser fluid evolves into fronts, one along the bed and the other in opposite direction. When the block of dense fluid is totally evolved into fronts the front distance travelled and front velocity shows accurate agreement with the analytical solution. Hence, from these simulation results it is concluded that conservation of momentum is satisfied within this discretised scheme.

Momentum balance
XXXXXXXXXXXXXXXXXXXXXXXXXXXXXXXXXXXXXXXXXXXXXXXXXXXXXXXXXXXXXXXXXXXXXXXX XXXXXXXXXXXXXXXXXXXXXXXXXXXXXXXXXXXXXXXXXXXXXXXXXXXXXXXXXXXXXXXXXXXXXXXX XXXXXXXXXXXXXXXXXXXXXXXXXXXXXXXXXXXXXXXXXXXXXXXXXXXXXXXXXXXXXXXXXXXXXX:

$$X = \frac{XX}{XX + XXX}$$

XXXXXXXXXXXXXXXXXXXXXXXXXXXXXXXXXXXXXXXXXXXXXXXXXXXXXXXXXXXXXXXXXXXXXXXX XXXXXXXXXXXXXXXXXXXXXXXXXXXXXXXXXXXXX.

XXXXXXXXXXXXXXXXXXXXXXXXXXXXXXXXXXXXXXXXXXXXXXXXXXXXXXXXXXXXXXXXXXXXXXXX XXXXXXXXXXXXXXXXXXXXXXXXXXXXXXXXXXXXXXXXXXXXXXXXXXXXXXXXXXXXXXXXXXXXXXXX XXXXXXXXXXXXXXXXXXXXXXXXXXXXXXXXXXXXXXXXXXXXXXXXXXXXXXXXXXXXXXXXXXXXXXXX XXXXXXXXXXXXXXXXXXXXXXXXXXXXXXXXXXXXXXXXXXXXXXXXXXXXXXXXXXXXXXXXXXXXXXXX XXXXXXXXXXXXXXXXXXXXXXXXXXXXXXXXXXXXXXXXXXXXXXXXXXXXX.

XXXXXXXXXXXXXXXXXXXX
XXXXXXXXXXXXXXXXXXXXXXXXXXXXXXXXXXXXXXXXXXXXXXXXXXXXXXXXXXXXXXXXXXXXXXXX XXXXXXXXXXXXXXXXXXXXXXXXXXXXXXXXXXXXXXXXXXXXXXXXXXXXXXXXXXXXXXXXXXXXXXXX XXXXXXXXXXXXXXXXXXXXXXXXXXXXXXXXXXXXXXXXXXXXXXXXXXXXXXXXXXXXXXXXXXXXXXXX XXXXXXXXXXXXXXXXXXXXXXXXXXXXXXXXXXXXXXXXXXXXXXXXXXXXXXXXXXXXXXXXXXXXXXXX XXXXXXXXXXXXXXXXXXXXXXXXXXXXXXXXXXXXXXXXXXXXXXXXXXXXXXXXXXXXXXXXX.

(a) (b)

[redacted]

Figure 6.15XXXXXXXXXXXXXXXXXXXXXXXXXXXXXXXXXXXXXXXXXXXXXXXXXXXXXXXXXXXXX

XXXXXXXXXXXXXXXXXXXXXXXXXXXXXXXXXXXXXXXXXXXXXXXXXXXXXXXXXXXXXXXXXXXXXXXXXXXXXXXXXXXXXXXXXXXXXXXXXXXXXXXXXXXXXXXXXXXXXXXXXXXXXXXXXXXXXXXXXXXXXXXXXXXXXXXXXXXXXXXXXXXXXXX.

Internal lock gate raise with deposition flux

Here we define the exact same lock gate raise problem as above however settling of sediment is included. Settling of suspended sediment will result in a decrease in concentration and therefore a decrease in the driving force (density difference) of the internal current. With this problem it is verified if the model remains stable if its driving force (density difference) approaches zero. As a consequence propagation of the internal current has to stop.

Figure 6.16 (a) shows the propagation of the density driven exchange current on different periods in time subjected to a deposition flux. Graph (b) shows the amount of concentration still trapped in the internal current on log scale.

(a)

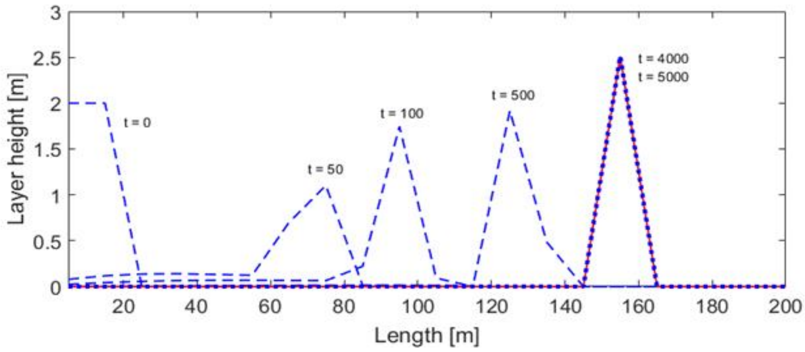

(b)

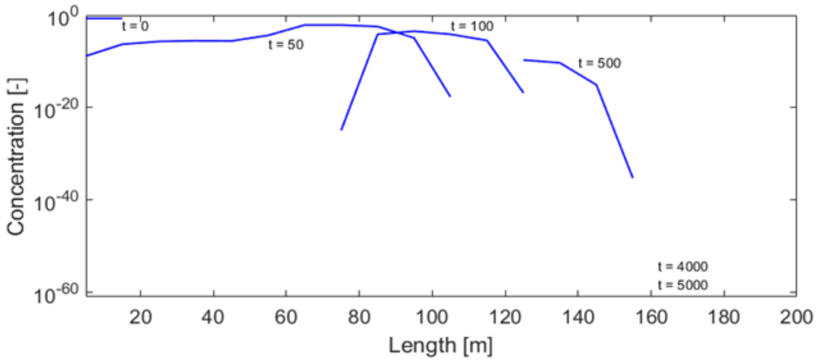

Figure 6.16 Graph a shows the propagation of the internal current after periods of respectively 0, 50, 100, 500, 4000 and 5000 s. Graph b shows the suspended sediment concentration trapped inside the internal current at the defined time periods on log scale.

When time elapses more sediment has settled and internal concentration approaches zero, as a consequence front propagation velocity approaches zero and eventually stops when concentration equals zero. Figure 6.16 shows that after a certain period (t = 4000, t = 5000 s.) the concentration in the density current is zero and front propagation stops.

6.5.2 Density current over a sloping bed

The density current propagates over a sediment bed which is certainly not perfectly horizontal. Bed gradients will result in acceleration or deceleration of the internal propagation and therefore it is highly important to verify this behaviour.

In this problem a block of dense fluid is situated on a sloping bed profile in a deep ambient water layer, h<<H. The block of dense fluid has an initial height and length of 3.0m and 100.0m respectively and the initial concentration of the block is 0.1 [-]. The bed slope is defined by a height to length ratio equal to 5/1000. The length of the domain is 1000m and the blob is initially situated in the middle of the domain.

Figure 6.17 shows the upward and downward propagation of fronts generated by the release of an initial block of dense fluid on a sloping bed. Different time periods are simulated to show the axial progression in time.

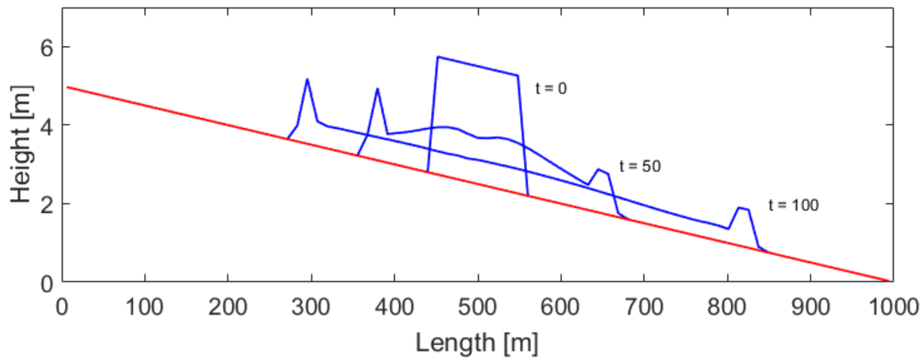

Figure 6.17 Front propagation in time of an initial block of dense fluid over a sloping bed. The graph shows snapshots of the fronts propagation upwards and downwards at periods t=0, t=50 and t=100.

XXXXXXXXXXXXXXXXXXXXXXXXXXXXXXXXXXXXXXXXXXXXXXXXXXXXXXXXXXXXXXXXXXXXXXXXXXXXXXXXXXXXXXXXXXXXXXXXXXXXXXXXXXXXXXXXXXXXXXXXXXXXXXXXXXXXXXXXXXXXXXXXXXXXXXXXXXXXXXXXXXXXXXXXXXXXXXXXXXXXX.

Conclusions based on case studies

Verification of the individual case studies as demonstrated above shows that the discretised numerical scheme for both the external as the internal water motion satisfies conservation of mass, momentum and mechanical energy. Furthermore the model can deal with drying and flooding phenomena and with transitions from subcritical to supercritical flow and vice versa at continues and discontinues bed gradients.

7 Model calibration and validation

In this chapter the developed 1D sedimentation model is validated against existing laboratory model experiments and prototype measurements (van Rhee, 2002). Firstly the sedimentation process is simulated with only the physics of the external (barotropic) hydrodynamic model, hence the effects of density currents is not considered in this approach. Thereafter, the density (internal) current is included (two-layered model) and these results are compared and calibrated with the experimental data. Most important parameters to predict within this model are the cumulative overflow losses and the bed level along the hopper length.

7.1 The hopper sedimentation process modelled with the external (barotropic) flow

Within this single-layer hydrodynamic model approach the internal flow is not included hence density currents do not contribute to horizontal suspended sediment transport.

Experimental model tests

The model scale hopper has the following dimensions, length of 12.0m, width of 3.07m and maximum overflow height of 2.25m, see Figure 7.1. The experimental setup, test program and model results are explicitly elaborated in (van Rhee, 2002).

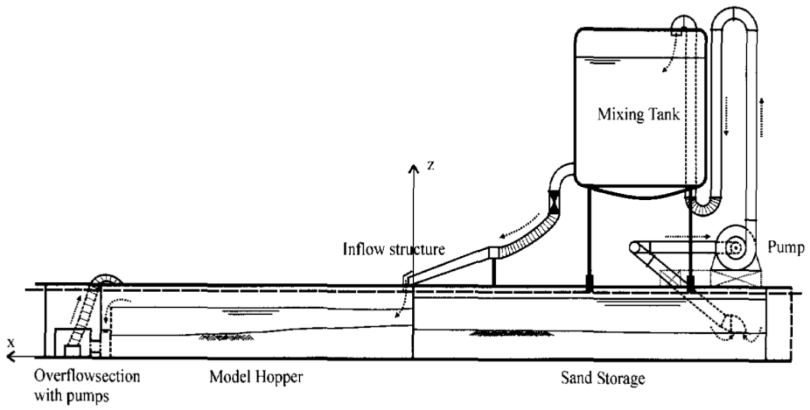

Figure 7.1 Experimental set-up hopper sedimentation tests (van Rhee, 2002).

The performance of this model is compared with several performed experiments (XXXXXXXXXXXXXXXX). These experiments are selected because they represent the largest mutually distribution in operational parameters. The operational parameters during these experiments are shown in Table 1 and Figure 7.2.

Table 1 Operational parameters during tests

	Test 05	Test 06	Test 08	Test 09	Test 12	Test 19
Discharge $[m^3/s]$	Xx	Xx	Xx	Xx	Xx	Xx
Density (average) $[kg/m^3]$	Xx	Xx	Xx	Xx	Xx	Xx
Overflow level [m]	Xx	Xx	Xx	Xx	Xx	Xx
Water level at start [m]	Xx	Xx	Xx	Xx	Xx	Xx
Bed level at start [m]	xx	xx	xx	xx	xx	xx

[redacted]

Figure 7.2 Operational parameters experimental tests (van Rhee, 2002)

The particle size distribution (PSD) of the inflowing (multi-sized) sand mixture as was measured in the model experiments is shown in Table 2:

Table 2 Particle size distribution as used in the tests

Particle Diameter [μm]	Cumulative Percentage [%]
xx	xx
xx	Xx
xx	Xx
Xx	Xx
Xx	Xx
Xx	Xx
Xx	Xx
xx	Xx

The particle size distribution as presented in Table 2 is used as input in the numerical model, hence the inflowing concentration is divided in seven different fractions with different particle diameter as presented above.

Overflow losses

The amount of overflowing sediments is described in terms of cumulative overflow losses, this parameter is defined as the ratio between the total sum of outflowing and inflowing sediment volume and is calculated as follows:

$$OV_{cum} = \frac{\int_0^t c_{ov}(t) Q_{ov}(t)\, dt}{\int_0^t c_{in}(t) Q_{in}(t)\, dt} \tag{6.24}$$

Where c_{ov} and c_{in} are respectively the overflow and inflow volumetric concentrations, Q_{ov} and Q_{in} represent the overflow and inflow amount of water/sediment mixture.

In the model hopper experiments the overflow concentration as well as the concentration in the hopper are measured during the entire loading process. Therefore the numerical model results are compared with the overflow concentration in time and the cumulative overflow losses.

Mass balance

The mass balance is continuously calculated during numerical simulations to verify the model satisfies conservation of mass. The mass balance is calculated for both water and solids by integration of the total inflowing discharge minus integration of the total overflowing discharge. When there is an initial water or bed layer in the hopper prior to a test this is also taken into account. The mass balance for solids reads:

$$M_{h\phi,end} = M_{h\phi,0} + \rho_s \int_{t=0}^{t_{end}} Q_{in} c_{in} dt - \rho_s \int_{t=0}^{t_{end}} Q_{out} c_{out} dt$$

Where $M_{h\phi,end}$ is the solids mass inside the hopper after loading, note that this can be both solids which forms the bed layer and solids in suspension. $M_{h\phi,0}$ is the solids mass inside the hopper prior to loading.

Influence of concentration in bed level growth on overflow losses

As explained in section 3.3 the presence of the concentration in the denominator of the bed level variation cannot be ignored with significant near bed concentrations. In Figure 7.3 & Figure 7.4 the influence of the near bed concentration in the bed level elevation expression is demonstrated for tests 5 and 6.

Figure 7.3: Measured and simulated (cumulative) overflow concentration for test 5.

Figure 7.4: Measured and simulated (cumulative) overflow concentration for test 6.

Both numerical simulations show that by including the concentration in the denominator (continuous blue dotted line) of the bed level elevation expression results in lower (cumulative) overflow losses. This is a logical result due to the increasing bed level elevation which results in more sediment extraction from the external layer. From the tests shown in Figure 7.3 & Figure 7.4 it is not obvious which approach results in more satisfying predictions within this single layer model approach.

Influence of particle size distribution

Horizontal transport of suspended sediment is derived from the one-dimensional horizontal advection equation. With the particle size distribution known in advance the sediment inflow flux is divided in a certain number of fractions. To calculate the horizontal transport of a single fraction the (1D) horizontal advection equation is explicitly solved for each single fraction as follows:

$$\frac{\partial \phi_{e,i} A_e}{\partial t} + \frac{\partial \phi_{e,i} A_e U_e}{\partial x} = (Source\ terms)_i \tag{6.25}$$

Where the term $\phi_{e,i}$ defines the concentration of a certain fraction (i) in the external layer and the source terms are defined in section 3.1.1. Vertical transport (settling) of each fraction is described by the effective settling velocity as was elaborated in Chapter 4.3. Note that vertical transport is not explicitly calculated within this model. Figure 7.5 and Figure 7.6 shows the comparison of simulations with multi-sized mixture and mono-sized (D_{50}) mixture.

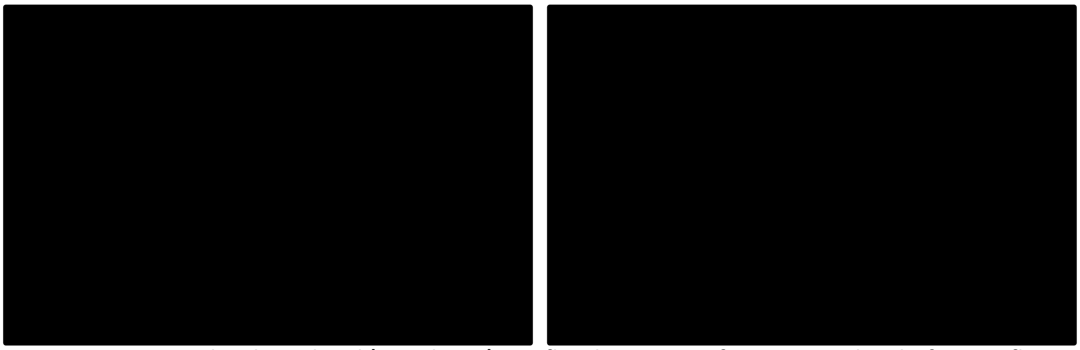

Figure 7.5: Measured and simulated (cumulative) overflow losses XXXX for mono- and multi-fraction flow.

[redacted] [redacted]

Figure 7.6: Measured and simulated (cumulative) overflow losses XXXX for mono- and multi-fraction flow.

Both Figures show that the multi-fractional flow (continuous blue dotted line) results in higher overflow losses compared to mono-sized flow (dashed blue line). This is a result of the lower settling velocity of the smaller fractions in the multi-sized mixture with respect to the courser particles in the mono-sized mixture. Therefore with a multi-sized mixture more sediment (fines particles) remains suspended.

Simulated cumulative overflow losses

Here the results of the numerical simulations of XXXXXXXXXXXX for cumulative overflow losses are compared with the measured results (red line). The inflowing mixture is subdivided in fractions (with the known PSD) to form a multi-sized mixture. The concentration is included in the denominator of the bed elevation rate (Eq. 3.55).

Test xx **Test xx**

[redacted] [redacted]

Test xx **Test xx**

[redacted] [redacted]

Figure 7.7: Simulation results of the cumulative overflow losses for XXXXXXXX.

Figure 7.7 shows that the total amount of overflowing solids is predicted well for Test 6. The simulated overflow losses in XXXXXXXX are over predicted within this (single layer) model. The simulated results for these tests is over predicted in the order of 0-10% compared to the measured results.

Appendix C shows the overflow concentration during time for the whole loading phase and the final bed level for the performed simulations. Note that the overflow concentration in time shows some difference compared to the measured results. A obvious recurring phenomenon is the over prediction of the overflow losses at the beginning of the overflow phase. This is mainly caused by the lack in vertical concentration distribution within this single layer model.

XXXXXXXXXXXXXXXXXXXXXXXXX
XXXXXXXXXXXXXXXXXXXXXXXXXXXXXXXXXXXXXXXXXXXXXXXXXXXXXXXXXXXXXXXXXXXXX XXXXXXXXXXXXXXXXXXXXXXXXXXXXXXXXXXXXXXXXXXXXXXXXXXXXXXXXXXX.

Test xx [redacted] **Test xx** [redacted]

Test xx [redacted] **Test xx** [redacted]

Figure 7.8: Simulation results of the bed level elevation in time for XXXXXX.

XXXXXXXXXXXXXXXXXXXXXXXXXXXXXXXXXXXXXXXXXXXXXXXXXXXXXXXXXXXXXXXXXXXXX XXXXXXXXXXXXXXXXXXXXXXXXXXXXXXXXXXXXXXXXXXXXXXXXXXXXXXXXXXXXXXXXXXXXX XXXXXXXXXXXXXXXXXXXXXXXXXXXXXXXXXXXXXXXXXXXXXXXXXXXXXXXXXXXXXXXXXXXXX XXXXXXXXXXXXXXXXXXXXXXXXXXXXXXXXXXXXXXXXXXXXXXXXXXXXXXXXXXXXXXXXXXXXX

XXXXXXXXXXXXXXXXXXXXXXXXXXXXXXXXXXXXXXXXXXXXXXXXXXXXXXXXXXXXXXXXXXXXXXXX
XXXXXXXXXXXXXXXXXXXXXXXXXXXXXXXXXXXXXXXXXXXXXXXXXXXXXXXXXXXXXXXXXXXXXXXX
XXXXXXXXXXXXXXXXXXXXXXXXXXXXXXXXXXXXXXXXXXXXXXXXXXXXXXXXXXXXXXXXXXXXXXXX
XXXXXXXXXXXXXXXXXXXXXXXXXXXXXXXXXXXXXXXXXXXXXXXXXXXXXXXXXXXXXXXXXXXXXXXX
XXXXXXXXXXXXXXXXXXXXXXXXXXXXXXXXXXXXXXXXXXXXXXXXXXXXXXXXXXXXXXXXXXXXXXXX
XXXXXXXXXXXXXXXXXXXXXXXXXXXXXXXXXXXXX.

[redacted]

Figure 7.9: Concentration/bed level in hopper during XXXX.

Comparison of cumulative overflow losses

In Figure 7.10 the measured and simulated cumulative overflow losses are compared. XXXXXXXXXXXXXXXXXXXXXXXXXXXXXXXXXXXXXXXXXXXXXXXXXXXXXXXXXXXXXXXXXXXXXXXX
XXXXXXXXXXXXXXXXXXXXXXXXXXXXXXXXXXXXXXXXXXXXXXXXXXXXXXXXXXXXXXXXXXXXXXXX
XXXXXXXXXXXXXXXXXXXXXXXXXXXXXXXXXXXXXXXXXXXXXXXXXXXXXXXXXXXXXXXXXXXXXXXX
XXXXXXXXXXXXXXXXXXXXXXXX.

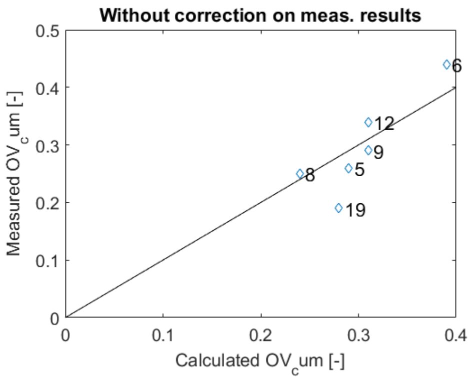

[redacted]

Figure 7.10 Measured versus simulated cumulative overflow losses.

XXXXXXXXXXXXXXXXXXXXXXXXXXXXXXXXXXXXXXXXXXXXXXXXXXXXXXXXXXXXXXXXXXXXXXXX
XXXXXXXXXXXXXXXXXXXXXXXXXXXXXXXXXXXXXXXXXXXXXXXXXXXXXXX.

Discussion 1D external (single layer) model

XXXXXXXXXXXXXXXXXXXXXXXXXXXXXXXXXXXXXXXXXXXXXXXXXXXXXXXXXXXXXXXXXXXXXXXX
XXXXXXXXXXXXXXXXXXXXXXXXXXXXXXXXXXXXXXXXXXXXXXXXXXXXXXXXXXXXXXXXXXXXXXXX

XXXXXXXXXXXXXXXXXXXXXXXXXXXXXXXXXXXXXXXXXXXXXXXXXXXXXXXXXXXXXXXXXXXXXXXXXXXX
XXXXXXXXXXXXXXXXXXXXXXXXXXXXXXXXXXXXXXXXXXXXXXXXXXXXXXXXXXXXXXXXXXXXXXXXXXXX
XXXXXXXXXXXXXXXXXXXXXXXXXXXXXXXXXXXXXXXXXXXXXXXXXXXXXXXXXXXXXXXXXXXXXXXXXXXX
XXXXXXXXXXXXXXXXXXXXXXXXXXXXXXXXXXXXXXXXXXXXXXXXXXXXXXXXXXXXXXXXXXXXXXXXXXXX
XXXXXXXXXXXXXXXXXXXXXXXXXXXXXXXXXXXXXXXXXXXXXXXXXXXXXXXXXXXXXXXXXXXXXXXXXXXX
XXXXXXXXXXXXXXXXXXXXXXXXXXXXXXXXXXXXXXXXXXXXXXX.

7.2 The hopper sedimentation process modelled with the external (barotropic) and internal (baroclinic) flow

Here the developed numerical model describing the sedimentation process including the effects of density currents is compared, calibrated and validated with the experimental model results and prototype measurements. The vertical sediment entrainment between the external- and internal current due to relative velocity difference is calibrated to the experimental results. Furthermore, the effects of internal erosion, the effect of including the concentration in the denominator of the bed level elevation expression and a correction to the deposition flux is examined. XXXXXXXXXXXXXXXXXXXXXXXXXXXXXXXXXXXXXXXXXXXXXXXXXXXXXXXXXXXXXXXXXXXXXX XXXXXXXXXXXXXXXXXXXXXXXXXXXXXXXXXXXXXXXXXXXXXXXXXXXXXXXXXXXXXXXXXXXXXX XXXXXXXXXXXXXXXXX.

The effects of density currents

By including the density current a "second" layer is included to the system and therefore the vertical concentration profile is divided into two separate layers. The density current causes some additional water and sediment fluxes to describe the transport between the external and internal layer. These processes are mentioned in section 3.1.1 and listed below:

- Sediment distribution at the inflowing mixture
- Sediment entrainment between external and internal layer
- Upward sediment flux due to upward flow velocity
- Upward water flux due to upward flow velocity
- External deposition flux into the internal layer

7.2.1 Sediment distribution at the inflowing mixture

The water sediment discharge entering the hopper propagates directly towards the bottom of the hopper due to buoyancy effects (Koning , 1977), (van Rhee, 2002). Therefore it is assumed the total mixture discharge directly forms a density current, hence no sediment is injected into the external current at the discharge location.

XXXXXXXXXXXX

XXXXXXXXXXXXXXXXXXXXXXXXXXXXXXXXXXXXXXXXXXXXXXXXXXXXXXXXXXXXXXXXXXXXXX XXXXXXXXXXXXXXXXXXXXXXXXXXXXXXXXXXXXXXXXXXXXXXXXXXXXXXXXXXXXXXXXXXXXXX XXXXXXXXXXXXXXXXXXXXXXXXXXXXXXXXXXXXXXXXXXXXXXXXXXXXXXXXXXXXXXXXXXXXXX XXXXXXXXXXXXXXXXXXXXXXXXXXXXXXXXXXXXXXXXXXXXXXXXXXXXXXXXXXXXXXXXXXXXXX XXXXXXXXXXXXXXXXXXXXXXXXXXXXXXXXXXXXXXXXXXXXXXXXXXXXXXXXXXXXXXXXXXXXXX XXXXXXXXXXXXXXXXXXXXXXXXXXXXXXXXXXXXXXXXXXXXXXXXXXXXXXXXXXXXXXXXXXXXXX XXXXXXXXXXXXXXXXXXXXXXXXXXXXXXXXXXXXXXXXXXXXXXXXXXXXXXXXXXXXXXXXXXXXXX XXXXXXXXXXXXXXXXXXXXXXXXXXXXXXXXXXXXXXXXXXXXXXXXXXXXXXXXXXXXXXXX..

7.2.2 XXXXXXXXXXXXXXXXXXXXXXXXXXXXXXXXXX

XXXXXXXXXXXXXXXXXXXXXXXXXXXXXXXXXXXXXXXXXXXXXXXXXXXXXXXXXXXXXXXXXXXXXX XXXXXXXXXXXXXXXXXXXXXXXXXXXXXXXXXXXXXXXXXXXXXXXXXXXXXXXXXXXXXXXXXXXXXX

XXXXXXXXXXXXXXXXXXXXXXXXXXXXXXXXXXXXXXXXXXXXXXXXXXXXXXXXXXXXXXXXXXXXXXX XXXXXXXXXXXXXXXXXXXXXXXXXXXXXXXXXXXXXXXXXXXXXXXXXXXXXXXXXXXXXXXXXXXXXXX XXXXXXXXXXXXXXXXXXXXXXXXXXXXXXXXX.

7.2.3 XXXXXXXXXXXXXXXXXX

XXXXXXXXXXXXXXXXXXXXXXXXXXXXXXXXXXXXXXXXXXXXXXXXXXXXXXXXXXXXXXXXXXXXXXX XXXXXXXXXXXXXXXXXXXXXXXXXXXXXXXXXXXXXXXXXXXXXXXXXXXXXXXXXXXXXXXXXXXXXXX XXXXXXXXXXXXXXXXXXXXXXXXXXXXXXXXXXXXXXXXXXXXXXXXXXXXXXXXXXXXXXXXXXXXXXX XXXXXXXXXXXXXXXXXXXXXXXXXXXXXXXXXXXXXXXXXXXXXXXXXXXXXXXXXXXXXXXXXXXXXXX XXXXXXXXXXXXXXXXXXXXXXXXXXXXXXXXXXXXXXXXXXXXXXXXXXXXXXXXXXXXXXXXXXXXXXX XXXXXXXXXXXXXXXXXXXXXXXXXXXXXXXXXXXXXXXXXXXXXXXXXX..

[redacted]

Figure 7.11: XXXXXXXXXXXXXXXXXXXXXXXXXXXXXXXXXXXXXXXXXXXXXXXXXXXXXXXXXXXXXXX.

XXXXXXXXXXXXXXXXXXXXXXXXXXXXXXXXXXXXXXXXXXXXXXXXXXXXXXXXXXXXXXXXXXXXXXX XXXXXXXXXXXXXXXXXXXXXXXXXXXXXXXXXXXXXXXXXXXXXXXXXXXXXXXXXXXXXXXXXXXXXXX XXXXXXXXXXXXXXXXXXXXXXXXXXXXXXXXXXXXXXXXXXXXXXXXX.

XXXXXXXXXXXXXXXXXXXXXXXXXXXXXXXXXXXXXXXXXXXXXXXXXXXXXXXXXXXXXXXXXXXXXXX XXXXXXXXXXXXXXXXXXXXXXXXXXXXXXXXXXXXXXXXXXXXXXXXXXXXXXXXXXXXXXXXXXXXXXX XXXXXXXXXXXXXXXXXXXXXXXXXXXXXXXXXXXXXXXXXXXXXXXXXXXXXXXXXXXXXXXXXXXXXXX XXXXXXXXXXXXXXXXXXXXXXXXXXXXXXXXXXXXXXXXXXXXXXXXXXXXXXXXXXXXXXXXXXXXXXX XXXXXXXXXXXXXXXXXXXXXXXXXXXXXXXXXXXXXXXXXXXXXXXXXXX.

[redacted]

Figure 7.12: Simulations of test5 with variation in erosion coefficient.

XXXXXXXXXXXXXXXXXXXXXXXXXXXXXXXXXXXXXXXXXXXXXXXXXXXXXXXXXXXXXXXXXXXX XXXXXXXXXXXXXXXXXXXXXXXXXXXXXXXXXXXXXXXXXXXXXXXXXXXXXXXXXXXXXXXXXXXX XXXXXXXXXXXXXXXXXXXXXXXXXXXXXXXXXXXXXXXXXXXXXXXXXXXXXXXXXXXXXXXXXXXX XXXXXXXXXXXXXXXXXXXXXXXXXXXXXXXXXXXXXXXXXXXXXXXXXXXXXXXXXXXXXXXXXXXX XXXXXXXXXXXXXXXXXXXXXXXXXXXXXXXXXXXXXXXXXXXXXXXXXXX These high erosion rates are caused by locally high flow velocities due to the relative steep slopes due to plateau formation, see Figure 7.13. Plateau's are formed when sediment with a certain sediment length scale settle, which results in increasing bed level. Beyond this particular sediment length scale less sediment settle and subsequently a bed slope develops.

[redacted]

Figure 7.13: Plateau formation

Propagation of the internal current over these relative steep bed gradients causes a local increase in flow velocity. When this flow velocity reaches the critical velocity erosion starts. Subsequently this can result in the erosion of the entire plateau. Hence by decreasing the erosion coefficient or by increasing the deposition flux plateau formation and subsequently erosion is intensified (amplitude of alternating pattern intensifies).XXXXXXXXXXXXXXXXXXXXXXXXXXXXXXXXXXXXXXXXXXXXXXXXXXXXXXX XXXXXXXXXXXXXXXXXXXXXXXXXXXXXXXXXXXXXXXXXXXXXXXXXXXXXXXXXXXXXXXXXXX XXXXXXXXXXXXXXXXXXXXXXXXXXXXXXXXXXXXXXXXXXX.

XXXXXXXXXXXXXXXXXXXXXXXXXXXXXXXXXXXXXXXXXX

XXXXXXXXXXXXXXXXXXXXXXXXXXXXXXXXXXXXXXXXXXXXXXXXXXXXXXXXXXXXXXXXXX XXXXXXXXXXXXXXXXXXXXXXXXXXXXXXXXXXXXXXXXXXXXXXXXXXXXXXXXXXXXXXXXXX XXXXXXXXXXXXXXXXXXXXXXXXXXXXXXXXXXXXXXXXXXXXXXXXXXXXXXXXXXXXXXXXXX XXXXXXXXXXXXXXXXXXXXXXXXXXXXXXXXXXXXXXXXXXXXXXXXXXXXXXXXXXXXXXXXXX XXXXXXXXXXXXXXXXXXXXXXXXXXXXXXXXXXXXXXXXXXXXXXXXXXXXXXXXXXXXXXXXXX XXXXXXXXXXXXXXXXXXXXXXXXXXXXXX.

[redacted]

Figure 7.14: XXXXXXXXXXXXXXXXXXXXXXXXXXXXXXXXXXXXXXXXX.

[redacted]

Figure 7.15: XXXXXXXXXXXXXXXXXXXXXXXXXXXXXXXXXXXXXXXXX.

XXXXXXXXXXXXXXXXXXXXXXXXXXXXXXXXXXXXXXXXXXXXXXXXXXXXXXXXXXXXXXXXXXXXXXXXXXXX XXXXXXXXXXXXXXXXXXXXXXXXXXXXXXXXXXXXXXXXXXXXXXXXXXXXXXXXXXXXXXXXXXXXXXXXXXXX XXXXXXXXXXXXXXXXXXXXXXXXXXXXXXXXXXXXXXXXXXXXXXXXXXXXXXXXXXXXXXXXXXXXXXXXXXXX XXXXXXXXXXXXXXXXXXXXXXXXXXXXXXXXXXXXXXXXXXXXXXXXXXXXXXXXXXXXXXXXXXXXXXXXXXXX XXXXXXXXXXXXXXXXXXXXXXXXXXXXXXXXXXXXXXXXXXXXXXXXXXXXXXXXXXXXXXXXXXXXXXXXXXX XXXXXXXXXXXXXXXXXXXXXXXXXXXXXXXXXXXXXXXXXXXXXXXXXXXXXXXXXXXXXXXXXXXXXX.

7.2.4 XXXXXXXXXXXXXXXXXX

XXXXXXXXXXXXXXXXXXXXXXXXXXXXXXXXXXXXXXXXXXXXXXXXXXXXXXXXXXXXXXXXXXXXXXXXXXXXX XXXXXXXXXXXXXXXXXXXXXXXXXXXXXXXXXXXXXXXXXXXXXXXXXXXXXXXXXXXXXXXXXXXXXXXXXXXX XXXXXXXXXXXXXXXXXXXXXXXXXXXXXXXXXXXXXXXXXXXXXXXXXXXXXXXXXXXXXXXXXXXXXXXXXXXX XXXXXXXXXXXXXXXXXXXXXXXXXXXXXXXXXXXXXXXXXXXXXXXXXXXXXXXXXXXXXXXXXXXXXXXXXXXX XXXXXXXXXXXXXXXXXXXXXXXXXXXXXXXXXXXXXXXXXXXXXXXXXXXXXXXXXXXXX.

[redacted]

Figure 7.16 Influence of entrainment flux on overflow losses and bed level elevation.

XXXXXXXXXXXXXXXXXXXXXXXXXXXXXXXXXXXXXXXXXXXXXXXXXXXXXXXXXXXXXXXXXXXXXXXXXXXXXX
XXXXXXXXXXXXXXXXXXXXXXXXXXXXXXXXXXXXXXXXXXXXXXXXXXXXXXXXXXXXXXXXXXXXXXXXXXXXXX
XXXXXXXXXXXXXXXXXXXXXXXXXXXXXXXXXXXXXXXXXXXXXXXXXXXXXXXXXXXXXXXXXXXXXXXXXXXXXX
XXXXXXXXXXXXXXXXXXXXXXXXXXXXXXXXXXXXXXXXXXXXXXXXXXXXXXXXXXXXXXXXXXXXXXXXXXXXXX
XXXXXXXXXXXXXXXXXXXXXXXXXXXXXXXXXXXXXXXXXXXXXXXXXXXXXXXXXXXXXXXXXXXXXXXXXXXXXX

XXXXXXXXXXXXXXXXXXXXXXXXXXXXXXXXXXXXXXXXXXXXXXXXXXXXXXXXXXXXXXXXXXXXXXX XXXXXXXXXXXXXXXXXXXXXXXXXXXXXXXXXXXXXXXXXXXXXXXX.

XXXXXXXXXXXXXXXXXXXXXXXXXXXXXXXXXXXXXXXXXXXXXXXXXXXXXXXXXXXXXXXXXXXXXXX XXXXXXXXXXXXXXXXXXXXXXXXXXXXXXXXXXXXXXXXXXXXXXXXXXXXXXXXXXXXXXXXXXXXXXX XXXXXXXXXXXXXXXXXXXXXXXXXXXXXXXXXXXXXXXXXXXXXXXXXXXXXXXXXXXXXXXXXXXXXXX XXXXXXXXXXXXXXXXXXXXXXXXXXXXXXXXXXXXXXXXXXXXXXXXXXXXXXXXXXXXXXXXXXXXXXX XXXXXXXXXXXXXXXXXXXXXXXXXXXXXXXXXXXXXXXXXXXXXXXXXXXXXXXXXXXXXXXXXXXXXXX XXXXXXXXXXXXXXXXXXXXXXXXXXXXXXXXXXXXXXXXXXXXXXXXXXXXXXXXXX.

7.2.5 XXXXXXXXXXXXXXXXXXX

XXXXXXXXXXXXXXXXXXXXXXXXXXXXXXXXXXXXXXXXXXXXXXXXXXXXXXXXXXXXXXXXXXXXXXX XXXXXXXXXXXXXXXXXXXXXXXXXXXXXXXXXXXXXXXXXXXXXXXXXXXXXXXXXXXXXXXXXXXXXXX XXXXXXXXXXXXXXXXXXXXXXXXXXXXXXXXXXXXXXXXXXXXXXXXXXXXXXXXXXXXXXXXXXXXXXX XXXXXXXXXXXXXXXXXXXXXXXXXXXXXXXXXXXXXXXXXXXXXXXXXXXXXXXXXXXXXXXXXXXXXXX XXXXXXXXXXXXXXXXXXXXXXXXXXXXXXXXXXXXXXXXXXXXXXXXXXXXXXXXXXXXXXXXXXXXXXX XXXXXXXXXXXXXXXXXXXXXXXXXXXXXXXXXXXXXXXXXXXXXXXXXXXXXXXXXXXXXXX.

XXXXXXXXXXXXXXXXX

XXXXXXXXXXXXXXXXXXXXXXXXXXXXXXXXXXXXXXXXXXXXXXXXXXXXXXXXXXXXXXXXXXXXXXX XXXXXXXXXXXXXXXXXXXXXXXXXXXXXXXXXXXXXXXXXXXXXXXXXXXXXXXXXXXXXXXXXXXXXXX XXXXXXXXXXXXXXXXXXXXXXXXXXXXXXXXXXXXXXXXXXXXXXXXXXXXXXXXXXXXXXXXXXXXXXX XXXXXXXXXXXXXXXXXXXXXXXXXXXXXXXXXXXXXXXXXXXXXXXXXXXXXX:

$$XX = XXXXXXXXXXXX \tag{7.26}$$

XXXXXXXXXXXXXXXXXXXXXXXXXXXXXXXXXXXXXXXXXXXXXXXXXXXXXXXXXXXXXXXXXXXXXXX XXXXXXXXXXXXXXXXXXXXXXXXXXXXXXXXXXXXXXXXXXXXXXXXXXXXXXXXXXXXXXXXX.

XXXXXXXXXXXXXXXXXXXXXXXXXXXXXXXXXXXXXXXXXXXXXXXXXXXXXXXXXXXXXXXXXXXXXXX XXXXXXXXXXXXXXXXXXXXXXXXXXXXXXXXX:

$$X = XXXXXX$$

XXXXXXXXXXXXXXXXXXXXXXXXXXXXXXXXXXXXXXXXXXXXXXXXXXXXXXXXXXXXXXXXXXXXXXX XXXXXXXXXXXXXXXXXXXXXXXXXXXXXXXXXXXXXXXXXXXXXXXXXXXXXXXXXXXXXXXXXXXXXXX XXXXXXXXXXXXXXXXXXXXXXXXXXXXXXXXXXXXXXXXXXXXXXXXXXXXXXXXXXXXXXXXXXXXXXX XXXXXXXXXXXXXXXXXXXXXXXXXX:

$$XX = XXXX \tag{7.27}$$

XXXXXXXXXXXXXXXXXXXXXXXXXXXXXXXXXXXXXXXXXXXXXXXXXXXXXXXXXXXXXXXXXXXXXXX XXXXXXXXXXXXXXXXXXXXXXXXXXXXXXXXXXXXXXXXXXXXXXXXXXXXXXXXXXXXXXXXXXXXXXX XXXXXXXXXXXXXXXXXXXXXXXXXXXXXXXXXXXXXXXXXXXXXXXXXXXXXXXXXXXXXXXXXXXXXXX XXXXXXXXXXXXXXXXXXXXXXXXXXXXXXXXXXXXXXXXXXXXXXXXXXXXXXXXXXXXXXXXXXXXXXX XXXXXXXXXXXXXXXXXXXXXXXXXXXXXXXXXXXXXXXXXXXXXXXXXXXXXXXX.

XXXXXXXXXXXXXXXXXX
XXXXXXXXXXXXXXXXXXXXXXXXXXXXXXXXXXXXXXXXXXXXXXXXXXXXXXXXXXXXXXXXXXXXXX XXXXXXXXXXXXXXXXXXXXXXXXXXXXXXXXXXXXXXXXXXXXXXXXXXXXXXXXXXXXXXXXXXXXXX XXXXXXXXXXXXXXXXXXXXXXXXXXXXXXXXXXXXXXXXXXXXXX.

XXXXXXXXXXXXXXXXXXXXXXX

[redacted]

Figure 7.17 XXXXXXXXXXXXXXXXXXXXXXXXXXXXXXXX.

XXXXXXXXXXXXXXXXXXXXXXXXXXXXXXXXXXXXXXXXXXXXXXXXXXXXXXXXXXXXXXXXXXXXXX XXXXXXXXXXXXXXXXXXXXXXXXXXXXXXXXXXXXXXXXXXXXXXXXXXXXXXXXXXXXXXXXXXXXXX XXXXXXXXXXXXXXXXXXXXXXXXXXXXXXXXXXXXXXXXXXXXXXXXXXXXXXXXXXXXXXXXXXXXXX XXXXXXXXXXXXXXXXXXXXXXXXXXXXXXXXXXXXXXXXXXXXXXXXXXXXXXXXXXXXXXXXXXXXXX XXXXXXXXXXXXXXXXXXXXXXXXXXXXXXXXXXXXXXXXXXXXXXXXXXX.

XXXXXXXXXXXXXXXXXXXXXXXXXXXXXXXXX

[redacted]

Figure 7.18: XXXXXXXXXXXXXXXXXXXXXXXXXXXXXXXXXXXXXX

XXXXXXXXXXXXXXXXXXXXXXXXXXXXXXXXXXXXXXXXXXXXXXXXXXXXXXXXXXXXXXXXXXXXX XXXXXXXXXXXXXXXXXXXXXXXXXXXXXXXXXXXXXXXXXXXXXXXXXXXXXXXXXXXXXXXXXXXXX XXXXXXXXXXXXXXXXXXXXXXXXXXXXXXXXXXXXXXXXXXXXXXXXXXXXXXXXXXXXXXXXXXXXX XXXXXXXXXXXXXXXXXXXXXXXXXXXXXXXXXXXXXXXXXXXXXXXXXXXXXXXXXXXXXXXXXXXXX XXXXXXXXXXXXXXXXXXXXXXXXXXXXXXXXXXXXXXXXXXXXXXXXXXXXXXXXXXXXXXXXXXXXX XXXXXXXXXXXXXXXXXXXXXXXXXXXXXXXXXXXXXXXXXXXXXXXXXXXXXXXXXXXXXXXXXXXXX XXXXXXXXXXXXXXXXXXXXXXXXX.

XXXXXXXXXXXXXXXXXXXXXXXXXXXXXXXXXXXXXXXXXXXXXXXXXXXXXXXXXXXXXXXXXXXXX XXXXXXXXXXXXXXXXXXXXXXXXXXXXX

[redacted]

Figure 7.19 Comparison of the measured and simulated total cumulative overflow losses.

XXXXXXXXXXXXXXXXXXXXXXXXXXXXXXXXXXXXXXXXXXXXXXXXXXXXXXXXXXXXXXXXXXXXX XXXXXXXXXXXXXXXXXXXXXXXXXXXXXXXXXXXXXXXXXXXXXXXXXXXXXXXXXXXXXXXXXXXXX XXXXXXXXXXXXXXXXXXXXXXXXXXXXXXXXXXXXXXXX.

Discussion of the two layer model

XXXXXXXXXXXXXXXXXXXXXXXXXXXXXXXXXXXXXXXXXXXXXXXXXXXXXXXXXXXXXXXXXXXXX XXXXXXXXXXXXXXXXXXXXXXXXXXXXXXXXXXXXXXXXXXXXXXXXXXXXXXXXXXXXXXXXXXXXX XXXXXXXXXXXXXXXXXXXXXXXXXXXXXXXXXXXXXXXXXXXXXXXXXXXXXXXXXXXXXXXXXXXXX XXXXXXXXXXXXXXXXXXXXXXXXXXXXXXXXXXXXXXXXXXXXXXXXXXXXXXXXXXXXXXXXX. XXXXXXXXXXXXXXXXXXXXXXXXXXXXXXXXXXXXXXXXXXXXXXXXXXXXXXXXXXXXXXXXXXXXX XXXXXXXXXXXXXXXXXXXXXXXXXXXXXXXXXXXXXXXXXXXXXXXXXXXXXXXXXXXXXXXXXXXXX XXXXXXXXXXXXXXXXXXXXXXXXXXXXXXXXXXXXXXXXXXXXXXXXXXXXXXXXXXXXXXXXXXXXX XXXXXXXXXXXXXXXXXXXXXXXXXXXXXXXXXXXXXXXXXXXXXXXXXXXXXXXXXXXXXXXXXXXXX XXXXXXXXXXXXXXXXXXXXXXXXXXXXXXXXXXXXXXXXXXXXXXXXXXXXXXXXXXXXXXXXXXXXX XXXXXXXXXXXXXXXXXXXXXXXXXXXXXXXXXXXXXXXXXXXX.

7.4.1 Validation against prototype data

A simulation of prototype measurements is performed to examine if the developed 1D model is capable to predict the amount of overflow losses and bed level along the hopper length on prototype scale. The measured prototype data on board of the TSHD "Cornelia" (van Rhee, 2002) is used as operational input for the simulation. Table 3 shows the dimensions of the hopper and the operational parameters, respectively.

Table 3: Geometrical dimensions and operational parameters "Cornelia"

Geometrical Dimensions Hopper		**Operational parameters**	
Vessel name	"Cornelia"	Discharge	6 $[m^3/s]$
Hopper length	52 $[m]$	Mixture density	1260 $[kg/m^3]$
Hopper width	11.5 $[m]$	Water density	1021 $[kg/m^3]$
Volume	5000 $[m^3]$	Porosity (bed)	0.46 [-]
Overflow height	8.36 $[m]$		

The average particle size distribution (PSD) as measured from samples taken from the seabed is shown below:

D_{10} $[\mu m]$	D_{20} $[\mu m]$	D_{30} $[\mu m]$	D_{40} $[\mu m]$	D_{50} $[\mu m]$	D_{60} $[\mu m]$	D_{70} $[\mu m]$	D_{80} $[\mu m]$	D_{90} $[\mu m]$
155	181	200	218	235	254	274	300	330

XXXXXXXXXXXXXXXXXXXXXXXXXXXXXXXXXXXXXXXXXXXXXXXXXXXXXXXXXXXXXXXXXXXXXX XXXXXXXXXXXXXXXXXXXXXXXXXXXXXXXXXXXXXXXXXXXXXXXXXXXXXXXXXXXXXXXXXXXXXX XXXXXXXXXXXXXXXXXXXXXXXXXXXXXXXXXXXXXXXXXXXXXXXXXXXXXXXXXXXXXXXXXXXXXX XXXXXXXXXXXXXXXXXXXXXXXXXXXXXXXXXXXXXXXXXXXXXXXXXXXXXXXXXXXXXXXXXXXXXX XXXXXXXXXXXXXXXXXXXXXXXXXXXXXXXXXXXXXXXXXXXXXXXXXXX.

Figure 7.20 shows the simulated results of the prototype simulation compared with the measured cumulative overflow losses. The results show that the numerical simulated overflow losses are of the same magnitude as the measured overflow losses on prototype scale. The simulated bed level profile cannot be compared with measured results because these results are not available.

(a)

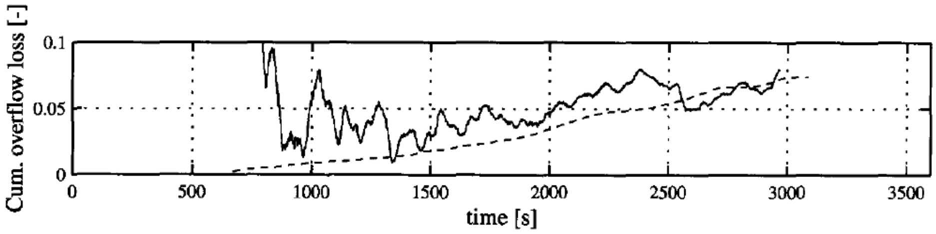

(b)

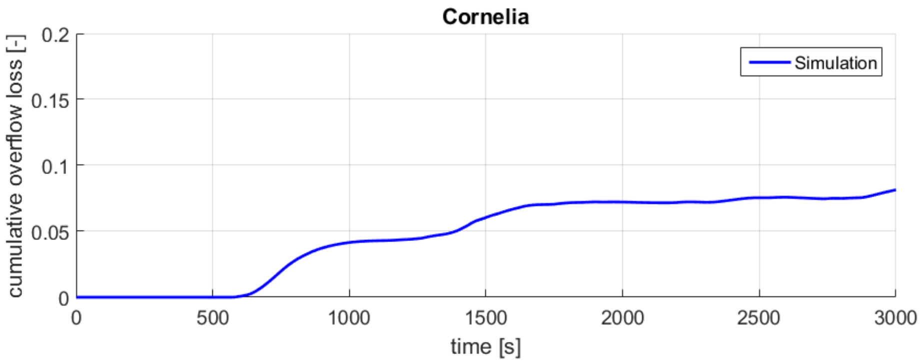

Figure 7.20: Results of simulating on prototype scale, graph (a) shows the measured cumulative overflow losses, graph (b) the numerical simulated cumulative overflow losses.

The measured total cumulative overflow losses are in the order of 0.075[-] whereas the measured losses has a value of 0.08[-]. Therefore it can be concluded that the developed and calibrated model can also predict the amount of overflow losses on prototype scale favourably well.

Comparison of measured and simulated cumulative overflow losses

Here the total cumulative overflow losses are compared with the measured overflow losses for the Tests and the prototype simulation.

Figure 7.21: Comparison of measured and simulated cumulative overflow losses

The coefficient of determination (R^2) for the cumulative overflow losses with the correct calibrated settings as used in the simulations is calculated to show the goodness of fit of the model. This value provides a measure how well the model reproduce observed outcomes. For the calculation of the coefficient of determination the R^2 value is calculated with the following definition:

$$R^2 = 1 - \frac{residual\ sum\ of\ squares}{total\ sum\ of\ squares} = 1 - \frac{\sum_i (y_i - f_i)^2}{\sum_i (y_i - \bar{y})^2} \tag{7.28}$$

Where y_i are the number of measured values, f_i are the number of simulated values and $\bar{y}$ is the mean of the measured data.

With the 7 performed simulations (experiments and prototype) for the total cumulative overflow losses as shown in Figure 7.21 the coefficient of determination has a value of $R^2 = 0.92$. This implies that the regression line (model) approximates the observed data favorably well.

8 Conclusions

This thesis describes the development, verification and validation of an one dimensional cross-sectional averaged numerical model to predict the sedimentation process inside the hopper. The emphasis of this research was to describe the physical processes occurring in the hopper within a one dimensional cross-section averaged approach to keep it tractable in calculation time and with low computational effort. The model is based on the layer averaged equations in conservative form. This hydrodynamic model is dynamically coupled with the sediment bed change through the effects of erosion and sedimentation. Furthermore this model contains the effects of density currents, configuration of in/outflow and hopper geometry within a cross-sectional averaged approach. The discretised hydrodynamic model is extensively verified against analytical solutions for both the external (barotropic) as well as the internal (baroclinic) current. It is demonstrated that the developed model can deal with drying/flooding processes and with transitions from sub- to supercritical flow and vice versa. Subsequently the model is calibrated and validated against model tests and prototype measurements of the hopper loading. The following conclusions can be drawn:

Hydrodynamic model

- Verification of the model to analytical solutions demonstrates the model is able to simulate the dynamical progression of free surface flows and axis-symmetric density currents (Section 6, page 42).
- XXXXXXXXXXXXXXXXXXXXXXXXXXXXXXXXXXXXXXXXXXXXXXXXXXXXXXXXXXXXXXXXXX XXXXXXXXXXXXXXXXXXXXXXXXXXXXXXXXXXXXXXXXXXXXXXXXXXXXXXXXXXXXXXXXXX XXXXXXXXXXXXXXXXXXXXXXXXXXXXXXXXXXXXXXXXXXXXXXXXXXXXXXXXXXXXXXXXXX XXXXXXX (Section **Error! Reference source not found.**, page **Error! Bookmark not defined.**).
- XXXXXXXXXXXXXXXXXXXXXXXXXXXXXXXXXXXXXXXXXXXXXXXXXXXXXXXXXXXXXXXXXX XXXXXXXXXXXXXXXXXXXXXXXXXXXXXXXXXXXXXXXXXXXXXXXXXXXXXXXXXXXXXXXX (Section **Error! Reference source not found.**, page **Error! Bookmark not defined.**).
- The model can deal with transitions from subcritical to supercritical flow and vice versa over continues and discontinues bed gradients (Section 6.2, page 48).
- Verification to analytical solutions shows that mass, momentum and energy are conserved within the external and internal currents (Section 6, page 52).
- XXXXXXXXXXXXXXXXXXXXXXXXXXXXXXXXXXXXXXXXXXXXXXXXXXXXXXXXXXXXXXXXXX XXXXXXXXXXXXXXXXXXXXXXXXXXXXXXXXXXXXXXXXXXXXXXXXXXXXXXXXXXXXXXXXXX XXXXXXXXXXXXXXXXXXXXXXXXXXXXXXXXXXXXXXXXXXXXXXXXXXXXXXXXXXXXXXXXXX XXXXXXXXXXXXXXXXXXXXXXXX (Section 6.5, page 59).

External (single layer) sedimentation model

- The external flow model can reasonably well predict the amount of overflow losses for the laboratory experiments (Section 7.1 , page 63).
- The influence of the concentration term in the denominator of the sedimentation velocity does not necessarily improve the results within the external flow model (Section 7.1, page 65).
- XXXXXXXXXXXXXXXXXXXXXXXXXXXXXXXXXXXXXXXXXXXXXXXXXXXXXXXXXXXXXXX XXXXXXXXXXXXXXXXXXXXXXXXXXXXXXX (Section 7.1, page 66).
- XXXXXXXXXXXXXXXXXXXXXXXXXXXXXXXXXXXXXXXXXXXXXXXXXXXXXXXXXXXXXXX XXXXXXXXXXXXXXXXXXXXXXXXXXXXXXXXXXXXXXXXXXXXXXXXXXXXXXXXXXXXXXX XXXXXXXXXXXXXXXXXXXXXXXXXXXXXXXXXXXXXXXXXXXXXXXXXXXXXXXXXXXXXXX XXXXXXXXXXXXXXXXXXXXXXXXX (Section 7.1, page 68).

External/Internal (two-layer) sedimentation model

- XXXXXXXXXXXXXXXXXXXXXXXXXXXXXXXXXXXXXXXXXXXXXXXXXXXXXXXXXXXXXXX XXXXXXXXXXXXXXXXXXXXXXXXXXXXXXXXXXXXXXXXXXXXXXXXXXXXXXXXXXXXXXX XXXXXXXXXXXXXXXXXXXXXXXXXXXX(Section 7.2.3, page 71).
- XXXXXXXXXXXXXXXXXXXXXXXXXXXXXXXXXXXXXXXXXXXXXXXXXXXXXXXXXXXXXXX XXXXXXXXXXXXXXXXXXXXXXXXXXXXXXXXXXX (Section 7.2.3 , page 71).
- Decrease of the erosion coefficient intensify the formation of plateau's in the bed level profile (Section 7.2.3, page 71).
- Bed level elevation in time shows an increasing trend superimposed with an alternating pattern. An explanation for this phenomenon is the erosion of plateau's. (Section 7.2.3, page 71).
- XXXXXXXXXXXXXXXXXXXXXXXXXXXXXXXXXXXXXXXXXXXXXXXXXXXXXXXXXXXXXXX XXXXXXXXXXXXXXXXXXXXXXXXXX (Section 7.2.3, page 73).
- XXXXXXXXXXXXXXXXXXXXXXXXXXXXXXXXXXXXXXXXXXXXXXXXXXXXXXXXXXXXXXX XXXXXXXXXXXXXXX (Section 7.2.5, page 76).
- XXXXXXXXXXXXXXXXXXXXXXXXXXXXXXXXXXXXXXXXXXXXXXXXXXXXXXXXXXXXXXX XXXXXXXXXXXXXXXXXXXXXXXXXXXXXXXXXXXXXXXXXXXXXXXXXXXXXXXXXXXXXXX XXXXXXXXXXXXXXXXXX (Section 7.2.5, page 78).
- XXXXXXXXXXXXXXXXXXXXXXXXXXXXXXXXXXXXXXXXXXXXXXXXXXXXXXXXXXXXXXX XXXXXXXXXXXXXXXXXXXXXXXXXXXXXXXXXXXXXXXXXXXXXXXXXXXXXX.
(Section 7.4.1, page 81).

This study demonstrates that the developed model can predict the amount of overflow losses and the longitudinal bed level elevation on model and prototype scale favourably well at a low user complexity level.

9 Recommendations

To further extend the developed model and to improve the results the following recommendations are presented:

- Derive more theoretical/experimental related values for the distribution factors describing water and sediment transport (XXXXXXXXXXXXXXX XXXXXXXXXXXXXXXXXXXXXXXXX) between the two layers.
- Include a 1DV model to more accurately predict the vertical suspended sediment profile to improve the deposition flux near the bed and the upward sediment flux between the internal and external layer.
- Perform more simulations on prototype scale for further validation of the numerical model and to quantify the pattern of bed level elevation.
- Include prototype simulations with silo- or keelson hopper shapes to show the influence of the cross-section hopper shape.

References

XXXXXXXXXXXXXXXXXXXXXXXXXXXXXXXXXXXXXXXXXXXXXXXXXXXXXXXXXXXXXXXXXX.

Bisschop, F., & van Rhee, C. (2010). Erosion due to high flow velocities: A description of relevant processes. *32nd International Conference on Coastal Engineering*.

Bonnecaze, R. (1993). *'Particle driven gravity current'.* Cambridge: Cambridge University Press.

XXXXXXXXXXXXXXXXXXXXXXXXXXXXXXXXXXXXXXXXXXXXXXXXXXXXXXXXXXXXXXXXXXX XXXXXXXXXXXXXXXXXXX.

C., V. R. (1993). *Principles of Sediment Transport in Rivers, Estuaries and Coastal Seas.* Amsterdam, The Netherlands .

Camp, T. (1946). Sedimentation and the design of settling tanks. *Trans. ASCE*, 895-936.

Ferguson, R., & Church, N. (2004). A simple universal equation for grain settling velocity. *Journal of sedimentary research* , 933-937.

XXXXXXXXXXXXXXXXXXXXXXXXXXXXXXXXXXXXXXXXXXXXXXXXXXXXXXXXXXXXXXXXXXX XXXXXXXXXXXXXXXXXXXXXXXXXXXXXXXXXXXXXX.

Hirsch, C. (2007). *Numerical computation of internal and external flows.* Oxford: John Wiley & Sons.

Koning , J. d. (1977). Constant loading system of trailing suction hopper dredgers. *Proc. Int. Course on modern dredging, Den Haag* .

Miedema, S. (2008). An analytical approach to the sedimentation process in trailing suction hopper dredgers. *Terra et Aqua 112*, 15-25.

Mirza, S., & Richardson, J. (1979). "Sedimentation of suspensions of particles of two or more sizes". *Chem. Eng. Sci. 34*, 447-454.

Nijs, M. A. (2010). *The 2DH modelling of turbidity currents generated by water injection dredging.* Wodcon 2010.

Pantin, H. (1979). *'Interaction between velocity and effective density in turbidity flow'.* Amsterdam: Elsevier Scientific Publishing company.

Pietrzak, J. (2015). *An introduction to stratified flows for civil and offshore engineers.* Delft: Dept. of Hydraulic Engineering TU Delft.

XXXXXXXXXXXXXXXXXXXXXXXXXXXXXXXXXXXXXXXXXXXXXXXXXXXXXXXXXXX.

XXXXXXXXXXXXXXXXXXXXXXXXXXXXXXXXXXXXXXXXXXXXXXXXXXXXXX

Richardson, J. a. (1954). Sedimentation and fluidization . *Trans. Inst. Chem. Eng.* , 32(35):112.

Rouse, H. (1938). *'Fluid Mechanics for hydraulic engineers' .* New York: McGraw-Hill.

Rowe, P. (1987). A convenient empirical equation for estimation of the Richardson-Zaki exponent. *Chem. Eng. Science*, 2795-2796.

XXXXXXXXXXXXXXXXXXXXXXXXXXXXXXXXXXXXXXXXXXXXXXXXXXXXXXXXXXXXXXXXXXXXXX XXXXXXXXXXXXXXXXXXXXXXXXXXXXXXXXXXXXXXX.

Stelling , G., Kernkamp, H., & Laguzzi, M. (1998). *Delft Flooding System: A powerfull tool for inundation assessment based upon a positive flow simulation.* Copenhagen: Proc. of the 3th Int. Conf. on Hydroinformatics.

XXXXXXXXXXXXXXXXXXXXXXXXXXXXXXXXXXXXXXXXXXXXXXXXXXXXXXXXXXXXXXXXXXXXXX XXXXXXXXXXXXXXXXXXXXXXXXXXXXXXXXXX

Van Rhee, C. (2010). Sediment Entrainment at High Flow Velocities . *Journal of Hydraulic Engineering vol. 118*, pp. 1236-1240.

van Rhee, P. C. (2002). *On the sedimentation process in a trailing suction hopper dredger.* Delft: TU Delft.

Van Rijn, L. C. (1993). *Principles of Sediment Transport in Rivers, Estuaries and Coastal Seas.* Amsterdam, The Netherlands.

Vlasblom, W., & Miedema, S. (1995). *A Theory for determining sedimentation and overflow losses in hoppers.* Amsterdam: 14th World Dredging Congress.

Xinya Ying, A. A. (2004). Upwind conservative scheme for the Saint Venant equations. *Hydraulic Engineering*, 977-987.

Yagi , T. (1970). Sedimentation effects of soil in hopper. *Proceedings 1st WODCON conference* .

XXXXXXXXXXXXXXXXXXXXXXXXXXXXXXXXXXXXXXXXXXXXXXXXXXXXXXXXXXXXXXXX XXXXXXXXXXXXXXXXXXXXXXXXXXXXXXXXXXXXXX.

A Appendix

First order diffusive behaviour (dam break)

The influence of the spatial step on the diffusive behaviour of the first order scheme is demonstrated in the figure below. This influence is shown for the dam beak problem as was elaborated in section 6. The results show the diminishing diffusive behaviour of the scheme with increasing number of nodes (N = 50, 100, 250 respectively).

(a)

[redacted]

(b)

[redacted]

(c)

[redacted]

(d)

[redacted]

(e)

[redacted]

(f)

[redacted]

Dam break over a dry bed

The problem of a propagating front due to a dam break over an initial dry bed requires some extra attention as explained in section 6.1. Figure A.1 shows the simulation after respectively 10 and 30 s. with the incorrect momentum discretisation for the dry bed approach. The results show that the velocity profile propagates much faster compared to the exact solution. Hence this discretised momentum scheme does not results in conservation of momentum.

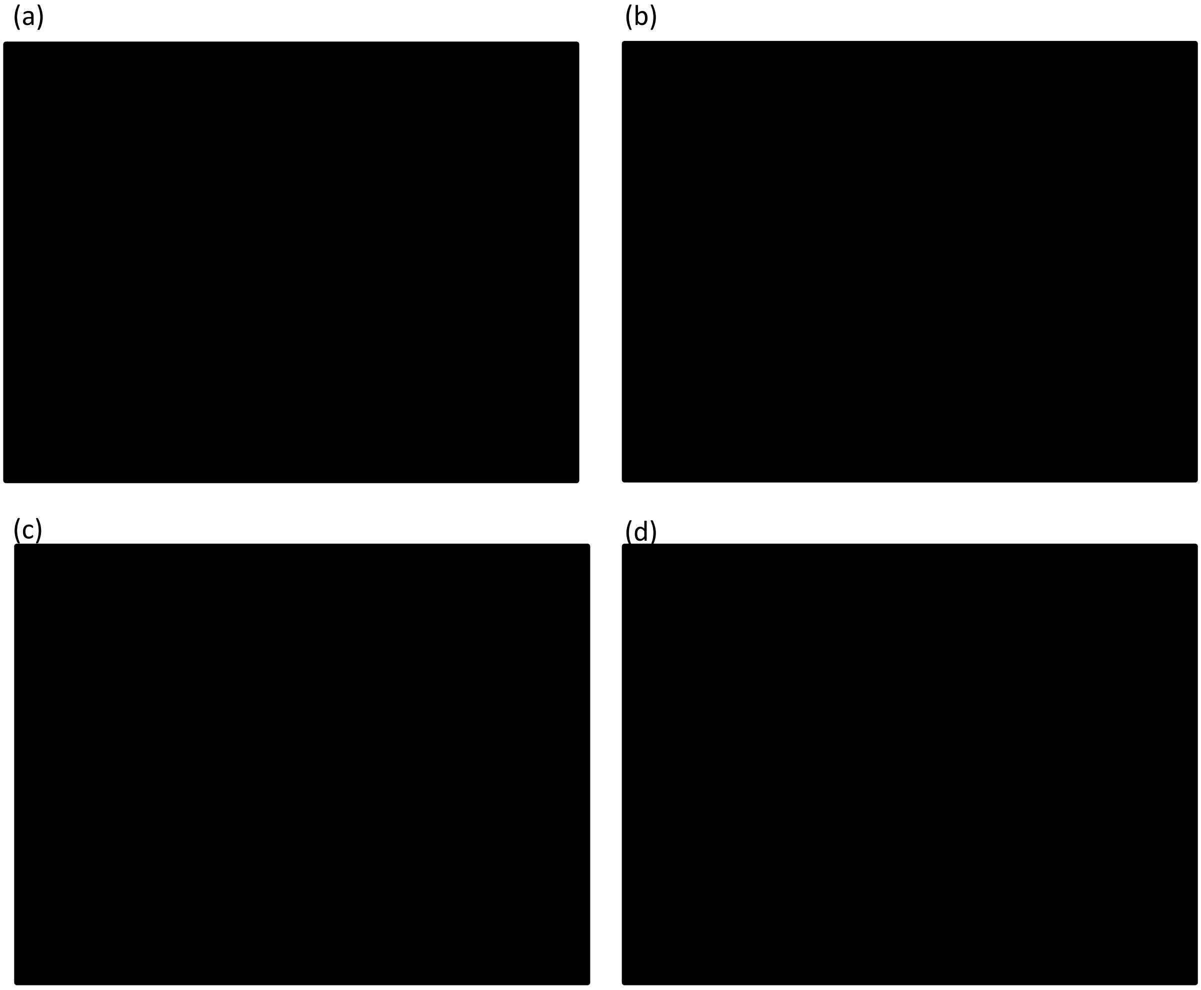

Figure A.1: Dam break with initial dry bed with incorrect momentum discretisation. Graph (a) shows water level and velocity profile after a simulation of 10 s., graph (b) shows water level and velocity profile after simulation of 30 s.

Hydraulic jump over a horizontal bed

The simulations below shows a hydraulic jump over a horizontal bed with different Froude numbers ($Fr^2 = 5, 10, 15, 20$) as was explained in section 6.2.

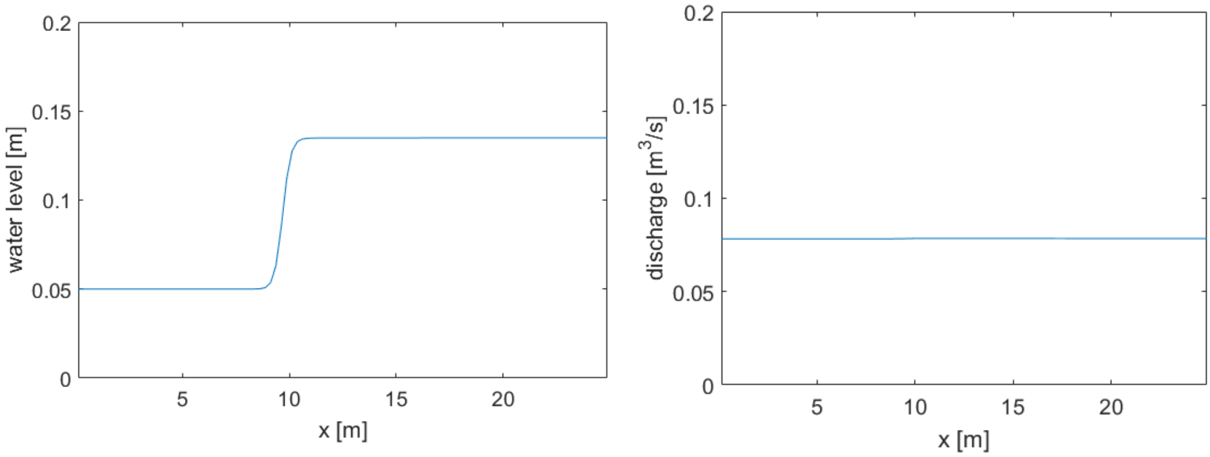

Figure A.2 Hydraulic jump simulation with downstream Froude number Fr1 = 5.

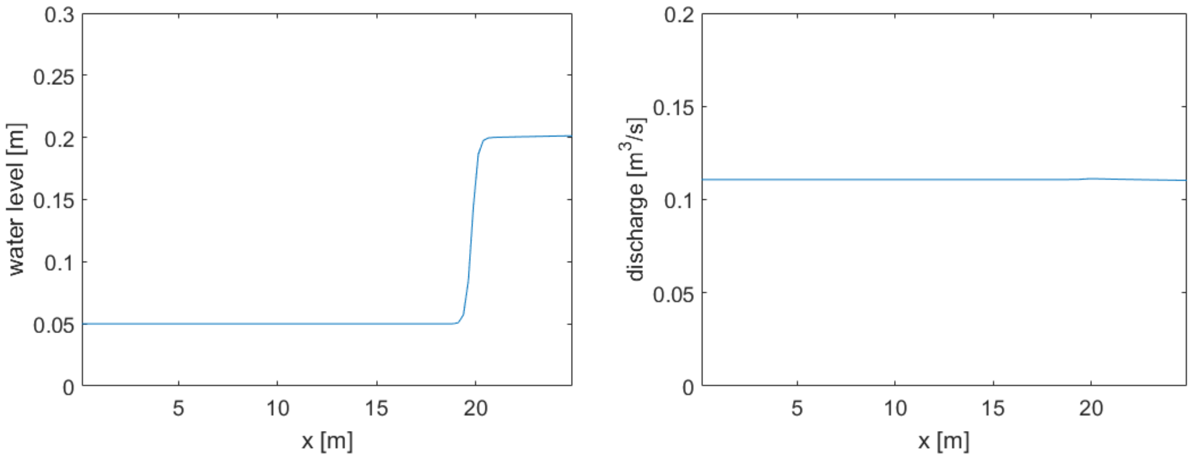

Figure A.4 Hydraulic jump simulation with downstream Froude number Fr1 = 10.

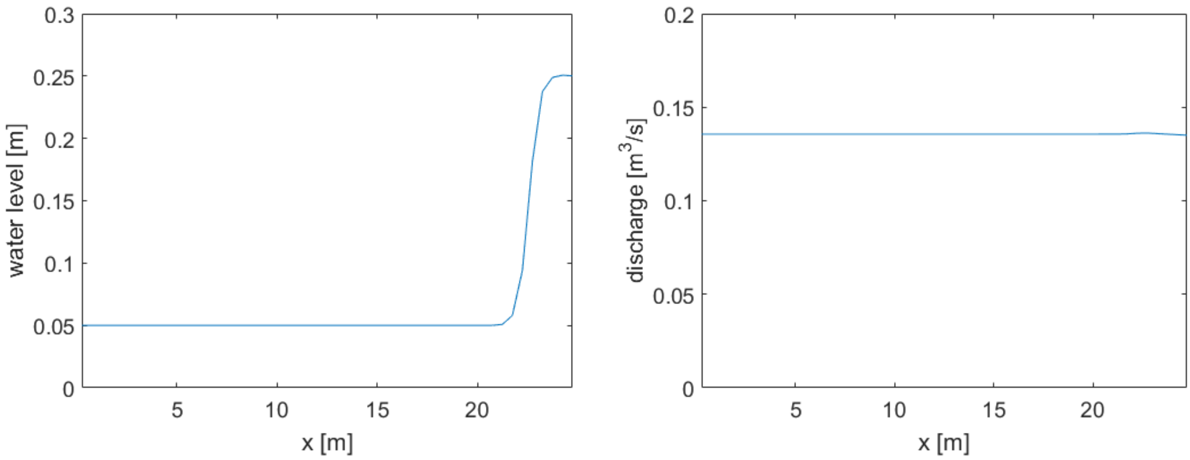

Figure A.3 Hydraulic jump simulation with downstream Froude number Fr1 = 15.

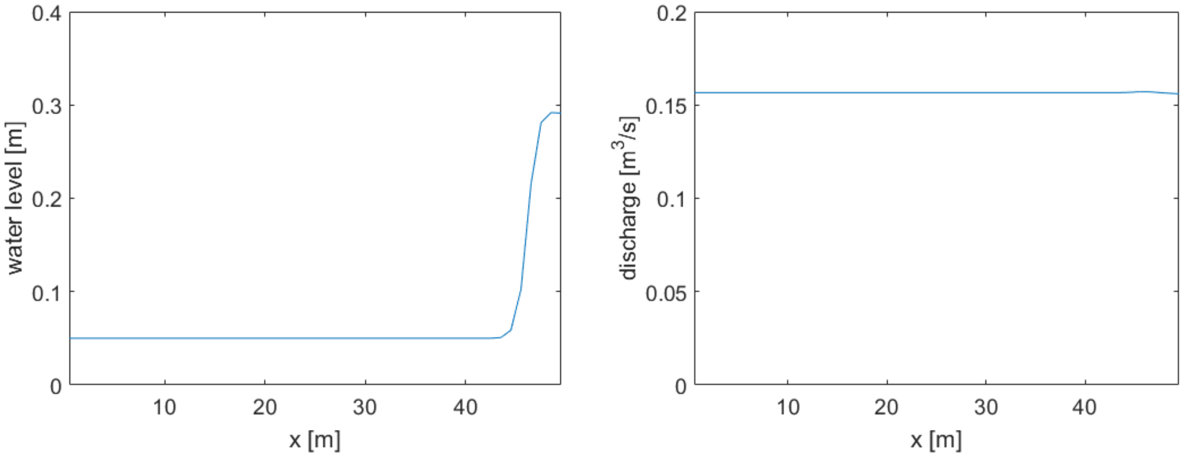

Figure A.5 Hydraulic jump simulation with downstream Froude number Fr1 = 20.

B Appendix

Here the results of the sedimentation model with the external flow only are presented and compared with the experimental measured results. The results show the overflow concentration in time, cumulative overflow losses in time, bed level elevation in time (at x = 3, 6, 9 m.) and the final bed level along the hopper.

Simulation results (external sedimentation process) test 5

Simulation results (external sedimentation process) Test 6

Simulation results (external sedimentation process) test 7

Simulation results (external sedimentation process) test 8

C Appendix

This appendix presents simulations of the sedimentation process with the external (barotropic) and internal (baroclinic) flow.

Here the influence of the concentration term in the sedimentation velocity expression is simulated for the two layered model.

<u>Concentration included in the sedimentation velocity expression</u>

No concentration in the sedimentation velocity expression

[redacted]

[redacted]

Influence of internal erosion

Firstly simulation without internal erosion are performed. This means only the external flow can cause erosion. Thereafter simulation with internal erosion are performed and variation in erosion coefficients show the influence of internal erosion on the bed level elevation in time and cumulative overflow losses.

<u>No internal erosion</u>

With internal erosion

[redacted]

[redacted]

D Appendix

Here the simulations of Tests 5, 6, 8, 9, 12, 13 with the calibrated settings are presented. The cumulative overflow losses, bed level elevation in time and the final bed level are presented. Note that there is still sediment in suspension at the end of the simulation. So the final bed level, especially at the overflow position (right side of domain) increases when the suspended sediment settles after some time. This will finally results in a higher bed level than shown in the simulations.

[redacted]

[redacted]